Overview of the Summer 2004 Intercontinental Chemical Transport Experiment-North America (INTEX-A)

H. B. Singh[1], W. H. Brune[2], J. H. Crawford[3], D. J. Jacob[4], and P. B. Russell[1]

1. NASA Ames Research Center, Moffett Field, CA 94035
2. Pennsylvania State University, PA 16902
3. NASA Langley Research Center, Hampton, VA 23665
4. Harvard University, MA 02138

Submitted to

Journal of Geophysical Research--Atmospheres
INTEX-A/ICARTT Special Section
August 2006

Abstract: The INTEX-A field mission was conducted in the summer of 2004 (July 1 to Aug. 15, 2004) over North America (NA) and the Atlantic in cooperation with multiple national and international partners. The main goals of INTEX-A were to (i) characterize the composition of the troposphere over NA; (ii) characterize the outflow of pollution from NA and determine its chemical evolution during transatlantic transport; (iii) validate satellite observations of tropospheric composition; (iv) quantitatively relate atmospheric concentrations of gases and aerosols with their sources and sinks; and (v) investigate aerosol properties and their radiative effects. INTEX-A primarily relied on instrumented DC-8 and J-31 aircraft platforms to achieve its objectives. The DC-8 was equipped to provide a detailed gas and aerosol measurement capability and provided sufficient range and altitude capability to coordinate activities with distant partners and to sample the entire mid-latitude troposphere. The J-31 was specifically focused on radiative effects of clouds and aerosols and operated largely in the Gulf of Maine. Satellite products along with meteorological and 3-D chemical transport model forecasts were integrated into the flight planning process. Inter-comparisons were performed to quantify the accuracy of data and to create a unified data set. Satellite validation activities principally focused on Terra (MOPITT, MODIS, and MISR), Aqua (AIRS and MODIS) and Envisat (SCIAMACHY) to validate satellite derived observations of CO, NO_2, HCHO, H_2O, and aerosol. Persistent fires in Alaska and NW Canada offered opportunities to quantify emissions from fires and study the transport and evolution of biomass burning plumes. Contrary to expectations, several pollution plumes of Asian origin, frequently mixed with stratospheric air, were sampled over NA. Quasi-lagrangian sampling was successfully carried out to study chemical aging of plumes during transport over the Atlantic.

Lightning NO_x source was found to be far larger than anticipated and provided a major source of error in model simulations. The composition of the upper troposphere was significantly perturbed by influences from surface pollution and lightning. CO_2 draw-down was characterized over NA and its atmospheric abundance related to terrestrial sources and sinks. INTEX-A observations provided a comprehensive data set to test models and evaluate major pathway of pollution transport over NA and the Atlantic. Major findings resulting from the initial analyses of INTEX-A observations are discussed. This overview provides a context within which the present and future INTEX-A/ICARTT publications can be understood.

1.0 Introduction

Rapid industrialization and the associated energy consumption have been major drivers of changes in atmospheric composition and climate [Houghton et al., 2001]. In recent decades a mounting body of atmospheric data have shown that gas and aerosol pollutants are routinely transported on intercontinental scales and can influence air quality and regional climate in downwind regions [Holloway et al., 2003; Stohl, 2004]. Independent studies have documented the transport of North American pollution to Europe [Stohl, A. and Trickl, 1999; Huntrieser et al., 2005; Derwent et al., 2006; Guerova et al., 2006]; Asian pollution to North America [Jaffe et al., 1999; Jacob et al., 1999; VanCuren, 2003]; Asian pollution to Europe [Lelieveld et al., 2002; Grousset et al., 2003], and North American and European pollution to Asia [Liu et al., 2002]. Observational data have shown that the surface O_3 mixing ratios of air entering Europe and NA may have increased by 0.3-0.5 ppb y^{-1} over the last two decades [Jaffe et al., 2003; Parrish et al., 2004; Simmonds et al., 2004; Vingarzan, 2004; Oltmans et al., 2006]. The direct and indirect radiative effects of aerosols on clouds are an equally urgent area of investigation [Seinfeld and Pandis, 1998; Houghton et al., 2001]. During the last decade the NASA* tropospheric chemistry program has investigated the outflow of pollution from the Asian continent to the Pacific Ocean [Hoell et al., 1996, 1997; Raper et al., 2001; Jacob et al., 2003]. INTEX-North America (NA) was a major NASA led integrated field experiment that focused on the inflow and outflow of pollution over the North American continent with the goal of understanding the transport and transformation of gases and aerosols on transcontinental/intercontinental scales [Singh et

al., 2002]. The first phase of INTEX-NA (INTEX-A) was completed in the summer of 2004 and forms the basis of this Special Section.

INTEX-A/ICARTT was an integrated mission that included multiple national and international partners (http://cloud1.arc.nasa.gov/intex-na/; http://www.al.noaa.gov/ICARTT/). This effort had a broad scope to investigate the transport and chemistry of long-lived greenhouse gases, oxidants and their precursors, aerosols and their precursors, as well their relationship with radiation and climate. NASA's DC-8 and J-31 were joined by aircraft from a large number of European and North American partners (Table 1) to explore the composition of the troposphere over NA and the Atlantic as well as radiative properties and effects of clouds and aerosols in a coordinated manner. An important new advance has been the launch of new satellite instruments that have the capability to map pollution in the troposphere on regional to global scales [Borrell et al., 2004; Schoeberl et al, 2004; Richter et al., 2005]. INTEX-A performed the dual role of validating satellite observations of tropospheric composition as well as integrating them with in-situ observations. Specific sampling goals were achieved with the aid of a state-of-the art modeling and meteorological support system that allowed targeted sampling of air parcels with desired characteristics.

INTEX-A/ICARTT was organized around a few major objectives aimed at (i) characterizing the large scale composition of the NA troposphere; (ii) characterizing the outflow of pollution from NA and determining its chemical evolution during transatlantic transport; (iii) validating satellite observations of tropospheric composition; (iv) quantitatively relating atmospheric concentrations of gases and aerosols with their

*Acronyms are provided in Appendix A

sources and sinks; and (v) investigating aerosol radiative properties and their effects. Summer season was selected as it is a season that is photochemically active, biogenic emissions and boreal fires are at their peak, and aerosol radiative forcing is near its maximum. Cold fronts and warm conveyor belts, while reduced in frequency in summer, continue to lift NA surface pollution to the free troposphere where it can be carried by the prevailing westerlies towards the European continent. INTEX-A aimed to better understand the chemical and physical processes that control the evolution of pollution during transatlantic transport, provide the advantage of improved source characterization offered by concurrent measurements of a large number of chemical species, relate radiative and chemical properties, and ultimately improve predictive capabilities via accurate model simulations.

Although several field experiments have been performed over NA in the past decades and results published and critically evaluated in special issues of journals [see Fehsenfeld et al., 1996; Penkett et al., 1998; Singh et al., 1999; Russell et al., 1999; Schere et al., 2000], this study was the most complex and integrated study done to date that spanned the mid-latitudes from the eastern Pacific to the eastern Atlantic and permitted sampling of the entire troposphere over NA. This overview focuses mainly on the goals and activities of the NASA DC-8 and J-31 aircraft during the summer 2004 study.

2.0 Mission Design and Implementation

2.1 Measurement platforms

The principal mobile platforms that participated in the INTEX-A/ICARTT campaign, their base of operation, campaign duration, and specifications are summarized in Table 1. Approximately 9 aircraft participated in this study for extended periods of time. One other aircraft (NSF Wyoming King Air) had a more limited role in this study and is not included in Table 1. These airborne platforms had the capability to sample much of the mid-latitude troposphere over long distances. The bases of operation were selected to facilitate sampling over NA and during transatlantic transport. Complementing these airborne platforms were several fixed surface air quality stations that operated during this study and in some cases continued to collect data after the study to develop more robust statistics. Principal among these were several air quality ground stations located in New Hampshire, Chebogue Point (Canada), and Pico (Azores). The NOAA ship R/V R H Brown also focused on the boundary layer outflow of pollution in the Gulf of Maine.

Additionally, data were available from several satellites overhead both in real time and for post mission analysis. Satellite observations both guided flight planning and helped to extend the range of airborne observations. In return, the airborne measurements provided validations of satellite observations. Integration of data from these multiple platforms was one of the central goals of this study. The INTEX Ozonesonde Network Study (IONS), organized by pooling resources from Environment Canada, NASA and NOAA, provided some 300 O_3 profiles from 11 fixed NA stations and the R/V R H Brown [Thompson et al., 2006]. The IONS network covered a wide region over NA that extended from 30 to 45˚N and 60 to 125˚W. Ozonesonde were released on a daily basis from three fixed sites and the R/V R H Brown and 1–3 times a week from other stations. Additional details about these platforms are available from

http://cloud1.arc.nasa.gov/intex-na/ and http://www.al.noaa.gov/ICARTT/ and have been further summarized by Fehsenfield et al. [2006].

2.2 Instrument payload and measurement capability

The payload of a majority of airborne platforms in Table 1 (e. g. DC-8, WP-3D, G-1, BAe-146, Falcon) was designed to measure detailed gas and aerosol composition in the troposphere. Three aircraft (J-31, Twin Otter, and Convair) were more focused on radiative and microphysical properties of clouds and aerosols. The DC-8 and the J-31 had an additional role that involved validation of satellite measurements of gases and aerosol optical properties in the troposphere. Table 2A shows the DC-8 payload of in situ and remote sensors for measurements of both gases and aerosols. Major greenhouses gases, ozone and precursors, aerosols and precursors, and a large number of tracers were measured in INTEX-A. Detailed VOC, OVOC, and reactive nitrogen (NO_x, HNO_3, HO_2NO_2, PAN) speciation was carried out. A large number of tracers that could be used to identify specific sources such as biomass combustion (HCN), biogenic emissions (isoprene), anthropogenic emissions (CO, halocarbons), and oceanic emissions ($CHBr_3$) were measured. A nadir and zenith viewing UV lidar measured O_3 and aerosols remotely. HO_x (OH and HO_2) free radicals, that are critical to understanding oxidative processes, were directly measured along with their precursors (peroxides and aldehydes). Spectral radiometers allowed direct measurement of actinic flux used to derive key photolysis frequencies. Detailed physical and chemical characterization of fine and coarse aerosol was carried out by multiple instruments aboard the DC-8. While many of the instruments had previously flown aboard the DC-8, several new instruments were incorporated. Two

new CIMS instruments were used to measure $HO_2NO_2$and SO_2 [Huey et al., this issue] and hydrogen peroxide [Crounse et al., 2006a]. A new LIF instruments measured NO_2 as well as total PANs and total alkyl nitrates via their thermal decomposition to NO_2 [Day et al, 2003]. INTEX-A provided the first in-situ measurements of HO_2NO_2 [Huey et al., this issue] and peracetic acid [Crounse et al., 2006b] in the troposphere.

Specific science objectives of the J31 included validating satellite retrievals of AOD spectra and of water vapor columns, measuring aerosol effects on radiative energy fluxes, and characterizing cloud properties using visible and near infrared reflectance in the presence of aerosols. To achieve these objectives, the J-31 carried two instruments (Table 2B) that operated in close coordination with measurements by other platforms especially the DC-8 and the R/V R H Brown. The Ames Airborne Tracking Sunphotometer (AATS) measured aerosol and water vapor attenuation of the direct beam from the Sun. The Solar Spectral Flux Radiometer (SSFR) measured solar energy from all directions with sensors looking both above and below the aircraft. Both AATS and SSFR covered a wide range of wavelengths, from the ultraviolet, through the visible, and into the near infrared.

Satellite instruments are becoming capable of air chemistry measurements in the troposphere and received a great deal of attention from the NASA DC-8 and the J-31 platforms. Principal focus in INTEX-A was on the CO vertical profiles obtained by AIRS and MOPITT, NO_2 and HCHO trop-columns from SCIAMACHY, and aerosol columns from MODIS-Terra, MODIS-Aqua, and MISR (Table 3). Additional details about the payloads of the platforms listed in Table 1 have been summarized in Fehsenfield et al. [2006]

2.3 Flight planning and execution

Satellite observations, along with meteorological and chemical forecasts from global and regional models were extensively used to plan, coordinate, and implement the INTEX-A field mission. Table 4 lists the major chemical transport models (CTMs) in use for planning this experiment. Meteorological products were derived from reanalysis data prepared by the National Centers for Environmental Prediction (NCEP) [Fuelberg et al., this issue]. Daily meteorological and chemical forecasts guided the design and execution of the mission. Typical model products included source-tagged CO tracers, aerosol tracers, O_3, and PAN distributions. Meteorological products included satellite imagery (visible, infrared, and water channels), precipitation and cloud fields, backward and forward trajectories and multi day synoptic weather forecasts. Principal satellite instruments that provided near real-time data to guide flight planning were AIRS and MOPITT (CO columns), SCIAMACHY (NO_2 columns), MODIS and AVHRR (aerosol, fire counts), and TOMS (tropospheric O_3, absorbing aerosols). To monitor lightning activity, real-time data from the National Lightning Detection Network (NLDN) and Long-Range Lightning Network (LRLN) were provided by the Global Hydrology and Climate Center at NASA Marshall Space Flight Center. These data were combined with forward trajectories by groups at Florida State and NASA Goddard to assess lightning influence for flight planning purposes.

The DC-8 science activities were closely coordinated with the main air quality (WP-3D, the BAe 146, and Falcon) and radiation (J-31) platforms. This coordination

was necessary to accomplish inter-comparisons among instruments, to achieve several objectives that were unattainable by a single platform, and to collect complementary data where appropriate. The bases of operation of these platforms (Table 1) were selected to sample NA atmospheric composition and transatlantic transport. In many cases quasi-lagrangian studies were carried out when pollution plumes sampled over NA were subsequently sampled over the central and eastern Atlantic after several days of transport [Law et al., 2005; Methven et al, 2006].

2.4 Flight tracks and sampled air masses

Figure 1A and 1B shows the flight tracks of four major air quality platforms (DC-8, WP-3D, BAe-146, Falcon-20) and the radiation platform (J-31) that collectively covered an area from the eastern pacific to the eastern Atlantic. Each flight was carefully planned to achieve the INTEX-A targeted objectives of investigating outflow of gases and aerosols, source characterization, chemical evolution, direct/indirect effects of aerosols, satellite validation, and instrument inter-comparisons. The DC-8 utilized a total of 170 available flight hours and conducted 2 test flights and 18 science flights (Dryden-2; Mid-America-6; and Pease-10) of 7-10 hour duration each from its three bases of operation (Table 5). As is evident from Figure 1 and Table 5A, the DC-8 started its activities from the west coast of U. S. and sampled air masses over the Pacific before moving to mid-America and ultimately joined other platforms at the eastern site. Figure 2 show the DC-8 flight tracks for each of the science flights. The J-31 utilized nearly 60 flight hours in shorter science flights of 2-4 hour duration operating exclusively from the New Hampshire site. Table 5A and 5B provide a brief summary of the flight objectives

of each of the DC-8 and J-31 flights with more details available at http://cloud1.arc.nasa.gov/intex-na/flight_reps.html. Figure 3 shows a plot of CO and O_3 that clearly shows that air masses influenced by forest fires, anthropogenic pollution, and stratosphere were sampled during INTEX-A.

2.5 Inter-comparisons

Intra- and inter-platform comparisons of measurements were a central theme in this experiment and these were extensively performed to establish accuracy and precisions. On the DC-8 itself, several chemical measurements were duplicated using a variety of different techniques (Table 2). Salient among these were measurements of O_3, H_2O, HCHO, H_2O_2, HNO_3, NO, and aerosol composition. Inter-comparisons were also performed with other aircraft by co-flying these in formation with a separation of less than 300 meters in the horizontal and 100 or so meters in the vertical. Two to 3 levels were chosen between 0 and 8 km altitudes and the entire inter-comparison including descent and ascent typically lasted one hour. Table 6 provides a summary of the inter-comparisons carried out by the DC-8. The BAe 146 intercompared with the DLR Falcon-20 based on the European continent. In short some level of intercomparison was available among all major ICARTT platforms. Figure 4 shows an example of such an inter-comparison for NO_2 and particle count. More details on inter-comparisons are provided elsewhere [http://www-air.larc.nasa.gov/missions/intexna/meas-comparison.htm].

2.6 Satellite validation

Satellites are increasingly able to measure key gases and aerosols in the troposphere. These sensors measure radiances from which information on atmospheric

composition is retrieved using inversions of radiative transfer algorithms, with substantial and often poorly characterized uncertainties. Validation with in situ vertical profiles is required, and this was a major activity during INTEX-A. The DC-8 focused on validation of CO, NO_2, H_2O, and HCHO, and together with J-31 on aerosols and clouds (Table 3). Opportunities for satellite validation were sought daily during flight planning. Figure 2 shows all the satellite spirals undertaken by the DC-8. Specific times and locations for these spirals are given in Table 7. Validations were performed to test retrievals with a variety of underlying surfaces. A typical DC-8 validation flight involved spiraling coincident with a satellite overpass to provide a full profile (and column) in the troposphere. Typically this meant measuring the troposphere between surface to 11.5 km in a spiral of about 20 km radius within ±30 minutes of the satellite overpass time under relatively cloud free conditions. This time coincidence was necessary for accurate validation and in addition provided a measurement of many chemical and physical parameters that could be used to improve satellite retrievals. In many cases it was possible to simultaneously validate multiple satellite sensors when the overpass times were similar and instrument swaths quite wide. In situ aerosol measurements on these DC-8 spirals have also been used to test aerosol retrievals from GOES [Kondragunta et al., this issue]. The satellite sensors of primary attention for the J-31 were MISR and MODIS (Table 3) and the focus was on validating satellite retrievals of aerosol optical depth (AOD) spectra and water vapor columns. Although the Aura satellite was launched in July 2004 and not ready for validation, it was possible to use INTEX-A data to set the stage for future TES/Aura validation [Zhang, et al., 2006].

3.0 Overview of First Results

We present here a brief overview and synthesis of the results presented in the first collection of INTEX-A/ICARTT papers assembled in this Special Section of Journal of Geophysical Research and published elsewhere to date. We primarily focus on the goals and activities of the NASA DC-8 and J-31 platforms. Complimentary papers are also being published in a second Special Section of Journal of Geophysical Research: ICARTT/NA-Europe. The reader is referred to the specific papers for more information.

3.1 Long distance transport of pollution

Fuelberg et al [this issue] provide an overview of the meteorological environment during INTEX-A. Anomalously strong and persistent high pressure over Alaska and western Canada brought unusually hot and dry conditions to that area. Seven cold fronts passed Atlanta, GA during INTEX-NA, the greatest number between 2000-2005. These fronts brought record low temperatures to portions of the Great Plains and South. Frontal passages over the Northeast were above average and the short time interval between passages (averaging 4.6 days) precluded the formation of stagnant high pressure centers that lead to pollution build up. The persistent high pressure over Alaska led to a record number of wildfires. The ridge also usually transported the fire by-products southeastward toward the INTEX-A domain where they were sampled by the DC-8 during numerous flights. On some flights, forward trajectories and satellite imagery showed that the plumes were also carried to parts of Europe, Africa, and the Arctic. The atmospheric chemistry during INTEX-A was heavily influenced by the record-breaking fires and the long-range transport of their by-products. An analysis of Cloud to Ground (CG) lightning from 2003-2005 showed that both flash counts and horizontal patterns of

lightning flashes during INTEX-NA were similar to other years. Deep convection and lightning were important factors during INTEX-NA. Analysis of data by Kiley et al. [this issue] shows that mid-latitude cyclones were capable of producing vertical transport as great or greater than much stronger cyclones.

3.1.1 Forest fire emissions and transport

The summer of 2004 was one of the largest fire seasons on record in North America, because of persistent wildfires in the boreal forests of Alaska and Canada resulting from exceptionally warm and dry conditions. According to the U.S. National Interagency Fire Center (http://www.cidi.org/wildfire), more than 2.6 million ha burned in Alaska in 2004, which represents more than 8 times the 10-year average and the highest burning on record, while the total area burned in the rest of the United States was only about 40% that of the 10-year average. In western Canada the fire season was well above the 10-year average, with 15 times the average area burned in the Yukon Territory (accounting for 60% of the national total) and 6 times the average area burned in British Columbia, according to the Canadian Interagency Forest Fire Center (CIFFC). Smoke plumes from these fires were identified by several satellites from their aerosol and CO signatures thousands of miles downwind and fire influences were widespread. As a result HCN and CH3CN, both tracers of biomass combustion, were elevated nearly everywhere in the troposphere [Singh et al., this issue]. The interception of biomass burning plumes several thousand kilometers downwind by the DC8 observations indicated that very limited mixing was occurring between the stretching filaments and the background. Tracers such as CO and HCN reached concentrations as high as 600 ppb and 3 ppb in mid

Atlantic. The smoke particles were also transported very efficiently from the source regions to Europe without major removal of particles. The availability of extensive atmospheric CO observations from aircraft and satellite for this period provided an opportunity to evaluate our understanding of factors controlling boreal fire emissions and their impact on atmospheric chemistry.

Turquety et al. [this issue] construct a daily bottom-up fire emission inventory, including consideration of peat burning and high-altitude (buoyant) injection, and evaluate it in a global chemical transport model (GEOS-Chem) simulation of CO through comparison with MOPITT satellite and ICARTT aircraft observations. They estimate a total NA fire emissions of 28.6 Tg-CO during the summer of 2004 consistent with the top-down estimate of 30 ± 5 Tg CO derived by Pfister et al. [2005] from inverse modeling of MOPITT observations. The fires represented a major perturbation to summertime North American emissions, of the same magnitude as the anthropogenic source (18 Tg CO). It is further deduced that the largest fires injected a significant fraction of their emissions in the upper troposphere that could be easily transported long distances.

Cook et al [2006] sought to investigate whether the fires in Alaska in 2004 were only of regional importance or had an impact on a wider, even hemispheric scale. They used the Cambridge TOMCAT model and the emissions data from Turquety et al. [this issue] and investigated the long-range transport of pollution across the North Atlantic and its impact on O_3 production. The simulated plumes closely match CO data from the aircraft and the MOPITT satellite instrument. Although uncertainties remain in the simulation of PAN and NO_x, TOMCAT simulations show increased O_3 in the troposphere

over much of NA, the north Atlantic and western Europe from photochemical production and transport. Biomass burning plumes sampled by the DC-8 in the free troposphere over NA did not show this O_3 enhancement. Hudman et al. [this issue] attribute this to rapid conversion of the emitted NO_x to PAN. They recommend that 85% of NO_x from boreal forest fires be emitted as PAN to the free troposphere in global CTMs.

McMillan et al. [this issue] focus on one major transport episode and investigate transport of CO from a large fire outbreak in the Alaskan/Canadian Yukon region on 11-14 July 2004 and follow it downwind to the southeastern United States and Europe until 22 July 2004. Correlations between AIRS CO and MODIS aerosol optical depths (AOD) indicate changes in the vertical distribution of CO as supported by in situ measurements, meteorological and forward trajectory analyses. Ground based lidar observations show smoke plume altitudes from 3 to 11 km over Wisconsin and 1 to 4 km over Maryland in agreement with the forward trajectories. Comparison of AIRS CO maps and forward trajectories from the fire locations illustrate the great variations in fire emissions, especially emission height, that must be accounted for if any forecast model is to correctly predict the impact of fire emissions days to weeks downwind.

Aerosol measurements revealed statistically robust differences in aerosol size, composition, spectral optical properties and humidity dependent growth for fires compared to other sources [Clarke et al., this issue]. Aerosol from fires were larger, had a greater fraction of organic carbon (OC) and had a lower growth in response to increasing humidity. They also exhibited unique spectral signatures that revealed that they could be separated optically using remote sensing approaches.

3.1.2 Asian Pollution over North America

Asian pollution transport to NA peaks in late spring and little influence in summer was expected. Contrary to this expectation, significant Asian pollution influences were encountered across NA. INTEX-A observations thus offered an unprecedented opportunity to quantify the role of transpacific transport of Asian pollution during summer. Asian air masses were identified via trajectory analysis, model simulations, and from their chemical composition. Liang et al. [this issue] identified five major Asian plumes sampled during INTEX-A and analyzed these observations to examine the summertime influence of Asian pollution in the free troposphere over NA. By applying correlation analysis and Principal Component Analysis (PCA) to the observations between 6-12 km, they find dominant influences from recent convection and lightning (13% of observations), Asia (7%), the lower stratosphere (7%), and boreal forest fires (2%), with the remaining 71% assigned to background. Typically Asian plumes contained high levels of CO, O_3, HCN, PAN, acetylene, benzene, methanol, and SO_4^{--}. The partitioning of reactive nitrogen species in the Asian plumes was dominated by PAN (~600 pptv), with varying NO_x/HNO_3 ratios in individual plumes consistent with different plume ages ranging from 3 to 9 days. Export of Asian pollution in warm conveyor belts of mid-latitude cyclones, deep convection, and lifting in typhoons all contributed to the five major Asian pollution plumes. Liang et al. [this issue] point out that compared to past measurement campaigns of Asian outflow during spring, INTEX-A observations display unique characteristics: lower levels of anthropogenic pollutants (CO, propane, ethane, benzene) due to their shorter summer lifetimes; higher levels of biogenic tracers (methanol and acetone) because of a more active biosphere; as well as higher levels of

PAN, NO_x, HNO_3, and O_3. The high $\Delta O_3/\Delta CO$ ratio (0.76 mol mol^{-1}) of Asian plumes during INTEX-A is suggested to be due to a combination of strong photochemical production and mixing with stratospheric air along isentropic surfaces.

3.1.3 North American pollution outflow and transatlantic transport

Air mass trajectories and model predictions were used to establish the occurrence of events where chemical processing could be studied in a quasi-Lagrangian framework. Several such opportunities were identified and aircraft successfully flown to the forecast locations of the previously sampled air masses. ICARTT studies provided evidence that this type of experiment can be successfully performed in the free troposphere on intercontinental scales. Attempts were made to intercept and sample air masses several times during their journey across the North Atlantic using four aircraft based in New Hampshire (USA), Faial (Azores) and Creil (France). Methven et al. [2006] describe techniques to identify Lagrangian matches between flight segments and further study five clear Lagrangian cases. They find indications of slow O_3 increases and CO decreases in the upper troposphere over the Atlantic.

Al-Saadi et al. [this issue] apply a novel technique for establishing source/receptor relationships to characterize the dominant contributions to O_3 distributions over the continental United States and Europe during the summer of 2004 campaign. They use Lagrangian trajectories to sample Eulerian fields from the global RAQMS model to establish source/receptor relationships based on geographic, chemical and meteorological criteria. For both United States and Europe they find that (1) approximately half the air in the lower troposphere experiences O_3 production within the domain upon exposure to

local precursor emissions, (2) air influenced by the stratosphere and by strong mixing has origins primarily over the Pacific Ocean 10 days earlier, and (3) exposure to high levels of PAN in the mid-tropospheric characterizes 20-25% of all free tropospheric air. The largest differences between United States and Europe were associated with persistent deep convection over the Gulf of Mexico and southern U.S. They find relatively little direct Asian influence on ozone over the U.S. during the summer of 2004 (2%) but a sizeable U.S. influence on Europe (9%).

3.2 Composition and Chemistry in the North American Troposphere

As can be seen from Figure 3, INTEX-A successfully characterized air masses of multiple origins over NA and the Atlantic at all different altitudes. A number of papers in this Special Section analyze and interpret these observations.

3.2.1 Ozone

Ozone was measured via in situ instruments and a UV lidar aboard the DC-8 as well as from coordinated ozonesonde launches from IONS (http://croc.gsfc.nasa.gov/intex/ ions.html>). The latter provided nearly 300 O_3 profiles from eleven North American sites and the R/V R H Brown in the Gulf of Maine [Thompson et al. this issue. 2006a,b]. Analysis of daily ozone soundings show that northeastern NA during INTEX-A was dominated by weak frontal systems that mixed aged pollution and stratospheric ozone with ozone from more recent pollution and lightning. These sources were quantified to give tropospheric ozone budgets for individual soundings. Cooper et al. [this issue] utilize data from daily ozonesondes, commercial aircraft, and lidar at 14 sites during July-August 2004 and find that the UT

above mid-latitude eastern NA contained 15-16 ppb more tropospheric residual ozone than the UT at the westerly upwind sites as well as the more polluted surface layers (0-2 km). Using observed data and simulations, they conclude that these O_3 enhancements can be generated from photochemical synthesis given significant amounts of lightning NO_x and only background mixing ratios of CO and VOCs.

3.2.2 Reactive nitrogen

INTEX-A provided the most detailed measurements of reactive nitrogen over the NA troposphere. Singh et al. [this issue] analyze the distribution and partitioning of this group of chemicals. They find that the North American upper troposphere was greatly influenced by both lightning NO_x and surface pollution lofted via convection and contained elevated concentrations of PAN, ozone, hydrocarbons, and NO_x. Under polluted conditions PAN was a dominant carrier of reactive nitrogen in the upper troposphere while HNO_3 dominated in the lower troposphere. Unknown Alkyl nitrates appear to be present in the continental boundary layer in moderately large concentrations. Horowitz et al. [this issue] suggest that isoprene nitrate may be a major contributor. Using a chemical ionization mass spectrometer (CIMS), Huey et al. [this issue] performed the first direct in situ measurements of HO_2NO_2 in troposphere. The highest mean HO_2NO_2 mixing ratios (76 ppt) were observed at altitudes of 8-9 km. with lower levels above and below. CTMs capture the broad structure of HO_2NO_2 but uncertainties among models are quite large. Aerosol nitrate appeared to be mostly contained in large soil based particles in the lower troposphere. Observational data suggested that lightning was a far greater contributor to NO_x in the upper troposphere than previously believed

and a major source of uncertainty among models [Hudman et al., this issue; Singh et al., this issue]. Dibb et al [this issue] use Beryllium-7 and the HNO_3/O_3 ratio to identify similar distinct stratospheric and tropospheric populations in the upper troposphere. Estimates based on ^7Be suggest that the stratosphere was a major source of HNO_3 in the UT. Hudman et al., [this issue] and Pierce et al. [this issue] calculate a NO_y export efficiency of 16% and 24% respectively from eastern NA using two different models.

3.2.3 HO_x, peroxides, and OVOC

Measurements of OH and HO_2 in INTEX-A provided an excellent test of atmospheric oxidation chemistry in and out of pollution plumes throughout the troposphere. Ren et al., [2006] compared OH and HO_2 measurements to predictions using a photochemical box model constrained by coincident measurements of long-lived tracers and physical parameters. For most of the troposphere, observed OH and HO_2 were less than expected from model calculations [Figure 5]. In the planetary boundary layer of forested regions, the observed-to-modeled OH ratio is a strong function of isoprene. The observed and modeled HO_2 greatly deviated in the UT (~2.5 at 11 km), suggesting either the presence of an unknown HO_x source or errors in model chemistry. These lower-than-expected OH measurements throughout much of the troposphere in northern midlatitudes have wide implications for ozone formation, global oxidation capacity, and reactive nitrogen distribution.

Peroxides and and formaldehyde were measured by two separate instruments [Crounse et al., 2006a; Fried et al., this issue; Snow et al. this issue]. Measurements of

peroxides also revealed the presence of peroxyacetic acid (PAA) which was quantified for the first time in INTEX-A. On several flights, the concentration of PAA in the upper troposphere exceeded that of hydrogen peroxide. Simulations using a constrained box model greatly underestimate the observed concentrations of PAA. In the upper troposphere, PAA was often 10-100 times larger than expected [Crounse et al., 2006b]. Unusually high concentrations of formaldehyde in the UT support the role of rapid convection that lofted HCHO from the lower troposphere [Fried et al., this issue]. Bertram et al. [this issue] find that convective outflow was strongest between 9 and 11 km and that more than 33% of the air in the UT had been placed there by convection within the last 2 days. Snow et al. [this issue] report considerable variability in mixing ratios of H_2O_2, CH_3OOH, and HCHO throughout the North American and North Atlantic troposphere. Convectively influenced air parcels were found to be enhanced in CH_3OOH, HCHO, CO, NO, and NO_2 while H_2O_2 and HNO_3 were depleted by wet removal. Biomass burning was also shown to increase upper troposphere H_2O_2, CH_3OOH, and HCHO mixing ratios even after 4-5 days of transit.

Oxygenated volatile organic compounds (OVOC) comprise a large number of the species whose transport to the remote troposphere can impact radical budgets, sequester NO_x in the form of nitrates, and play a role in the formation of organic aerosols. Kwan et al. [2006] use measurements of atmospheric oxidants and aerosol size distributions performed on the DC-8 during INTEX-A to suggest that organic aerosol oxidation by OH can be a significant source of OVOC in the troposphere. They estimate that the potential magnitude of OVOC flux from organic aerosol to be as large as 70 ppt C/day in the free troposphere. The potential importance and highly uncertain nature of these estimates

highlight the need for field and laboratory studies on organic aerosol composition and aging.

3.2.4 Aerosols and radiation

Clarke et al. [this issue] performed thermal analysis of aerosol size distributions and found that the "non-plume" regional haze was dominated by pollution characteristics near the surface and biomass burning aloft. Volatile OC included most water-soluble organic carbon. Refractory OC (stable at 400ºC) dominated the enhanced shortwave absorption in plumes from Alaskan and Canadian forest fires. Biomass burning, pollution and dust aerosol could be stratified by their combined spectral scattering and absorption properties. The measured response in light scattering to humidity revealed that ambient AOD typically included a 30-50% contribution from water due to its hygrosopicity.

Dry aerosol mass measured on the lowest flight legs provided an estimate of PM2.5, such as would be measured at the surface. Shinozuka et al. [this issue] show that ambient column AOD is well correlated (R^2=0.74) to near surface PM2.5 for most cases. This indicates satellite measurements of AOD could be used as a surrogate for PM2.5 for regions over NA where such measurements are not currently available. A related study by Kondragunta et al., (this issue) demonstrated that GOES AODs capture variability in atmospheric aerosol loading and can be used as a proxy to monitor pollution associated with urban/industrial sources and biomass burning events.

Other INTEX-A measurements of aerosols and radiation from the J-31 have been reported by Redemann et al. [2006]. They found high variability in the derived aerosol forcing efficiencies for the visible wavelength range (350-700 nm). They also estimated

aerosol absorption by matching calculations with the measured gradients of aerosol optical depth and radiant flux. In this way they found larger aerosol absorption early in the 12 July-8 August period than later, consistent with independent trajectory analyses and satellite imagery that showed the stronger influence of smoke aerosols from Alaska fires during the early period.

3.2.5 Carbon cycle and CO_2

North American terrestrial ecosystems are major sources and sinks of carbon. Quantifying their role in the continental carbon budget was a key objective in INTEX-A. Highly precise (±0.25 ppm), fast-response (1-s) measurements of CO_2 were obtained aboard the NASA DC-8 during INTEX-A. These measurements provided extensive regional-scale information on carbon sources and sinks over sparsely sampled areas of NA and adjacent ocean basins. Choi et al., [this issue] and Vadrevu et al. [this issue] use airborne and satellite data along with models to investigate the ecosystem-atmospheric CO_2 exchange over NA and its relationship with the observed atmospheric variability of CO_2 resulting from biospheric uptake, industrial activity, and atmospheric dynamics (Figure 6). Several products derived from the LANDSAT, NOAA AVHRR, and MODIS sensors were assimilated to specify spatiotemporal patterns of land use cover and vegetation characteristics to link the aircraft CO_2 data with terrestrial sources of carbon. They find that the lowest CO_2 mixing ratios were over agricultural fields in IL dominated by corn, a C_4 plants having a higher photosynthetic rate. The role of convection, strat-trop exchange, localized sources (e.g. power plants), and long-range transport on CO_2 spatial variability throughout the tropospheric column has been explored.

To facilitate and test column measurements of CO_2 from ground-based and space-borne instruments, the DC-8 and The University of Wyoming King Air aircraft (S. Wofsy, Harvard, concurrent COBRA campaign) recorded eight in situ CO_2 profiles over the Park Falls Wisconsin WLEF Tall Tower Site (45.945°N, 90.273°W) where an automated solar observatory for measuring atmospheric column abundances of CO_2 is co-located. Comparison of the integrated aircraft profiles and ground-based CO_2 column abundances (Figure 6) show excellent correlation but a small bias (~2%) [Washenfelder et al. 2006]. The comparison to aircraft integrated columns allowed the retrievals (CO_2 6228 cm^{-1} and 6348 cm^{-1}) to be corrected reducing the uncertainty in retrieved column-average CO_2 VMR to ~0.3% (±1.1 ppm).

3.3 Integrated Model Analysis of INTEX-A Observations and Model Evaluations

INTEX-A provided a vast amount of observational data that was further analyzed with the help of a variety of models of chemistry and transport [Table 4]. Figure 7 shows a comparison of the observed O_3 to NO_y ratio and its simulation by four state of the art models over a large grid over eastern NA (30-50°N; 260-320°W). It is evident that models disagree substantially with observations as well as with each other. Validation of existing models and their further improvement using INTEX-A data was a key focus in this campaign.

3.3.1 Synthesis of results using 3-D models

Pierce et al., [this issue] performed global ozone analyses, based on assimilation of stratospheric profile and ozone column measurements, and NO_y predictions from the

RAQMS model to estimate the ozone and NO_y budget over the Continental US. Comparison with available observations show that RAQMS captured the main features of the global and continental US distribution of tropospheric ozone, CO, and NO_y with reasonable fidelity. This study suggests that the majority of the Continental US export occurred in the upper troposphere/lower stratosphere pole-ward of the tropopause break. Continental US photochemically produced ozone was found to be a small component of the total ozone export, which was dominated by stratospheric ozone during INTEX-A. The NO_y export efficiency was estimated to be 24%, with NO_x and PAN together accounting for half of the total NO_y export.

Hudman et al. used the GEOS-Chem model to test current understanding of the regional budget of reactive nitrogen. They find that a 50% reduction in power plant and industry NO_x emissions over the Eastern United States between 1999-2004 due to the NO_x SIP Call resulted in estimated ozone decreases of 1-6 ppb. Increasing the model lightning source to match the constraints of observed NO_x had a 5-10 ppb positive impact on free tropospheric O_3 but led to a significant overestimate of OH. A Lagrangian analysis of the fraction of North American emissions vented to the free troposphere using NO_y-CO correlations indicated an NO_y export fraction of 15±10% consistent with previous studies but significantly lower than those estimated by Pierce et al., [this issue]. Contrary to previous studies, they find that PAN was by far the dominant component of NO_y (>50%) in pollution plumes above 3.5 km.

Horowitz et al [this issue] used a CTM simulation in conjunction with INTEX-A total alkyl nitrate and isoprene observations over the eastern United States to constrain uncertainties in the chemistry of isoprene nitrates. The best agreement between simulated

and observed boundary layer concentrations of organic nitrates were obtained with a 4% yield of isoprene nitrate production from the reaction of isoprene hydroperoxy radicals with NO, recycling of 40% NO_x when isoprene nitrated react with OH, and fast dry deposition of isoprene nitrates. Isoprene nitrates were shown to have a major impact on the NO_x budget in the continental boundary layer, consuming 17-21% of the emitted NO_x, with 3-6% being recycled back to NO_x and the remainder being exported as isoprene nitrates or deposited.

Pfister et al. [this issue] tested the MOZART-4 model with aircraft measurements and examined the ozone production from a case study of wildfires in Alaska and Canada. Modeled and observed enhancement ratios ($\Delta O_3/\Delta CO$) are about 0.25 ppb/ppb and result in a global net ozone production of 13±2 TgO_3 during summer 2004 in good agreement with the net ozone production calculated in the model for a region ranging from Alaska to the East Atlantic (9–11 Tg O_3). On average, the fires increased the ozone burden (surface– 300 hPa) over Alaska and Canada during summer 2004 by about 7–9%, and over Europe by about 2–3%.

3.3.2 Model evaluations:

Yu et al. [this issue] tested the performance of Eta-CMAQ model forecast performance with the observations obtained in this campaign. The model was able to capture the observed daily maximum 8-hr O_3 within a factor of 1.5 but underestimated CO by ~30% likely due to inadequate representation of the transport of pollution associated with Alaska forest fires. Chai et al., assimilate various O_3 measurements during INTEX-A/ICARTT into the STEM regional CTM and evaluate the effects of

assimilating O_3 observations on model predictions. During the operational phase of the ICARTT field experiment in 2004, the regional air quality model STEM showed a strong positive surface bias, and a negative upper troposphere bias with respect to ozone [Mena-Carrasco et al., this issue]. After updating emissions from NEI 1999 to NEI 2001 (with a 2004 large point sources inventory update), and modifying boundary conditions, surface model bias was essentially eliminated. Observed and modeled ozone production efficiencies (7.8) were in good agreement suggesting that the recurring ozone bias was due to overestimated NO_x emissions. Tarasick et al. [2006] compared ozonesonde O_3 data with O_3 profiles predicted by the Environment Canada CHRONOS and AURAMS forecast models. Although predictions of O_3 in the planetary boundary layer and immediately above were good, neither model was able to reproduce the typical profile of increasing mixing ratio with altitude. Chatfield et al. [this issue] interpret INTEX-A observations to develop an "index" that provides an empirical view of those factors most favoring ozone production.

3.4 Satellite Validation During INTEX-A

Figure 2 shows all the satellite spirals undertaken by the DC-8 during INTEX-A to validate principally AIRS (Aqua), MOPITT (Terra), and SCIAMACHY (Envisat) for CO, HCHO, NO_2, O_3 and H_2O. The three satellite sensors of primary attention for the J-31 were MISR on Terra, MODIS on Terra, and MODIS on Aqua and the focus was on validating satellite retrievals of aerosol optical depth (AOD) spectra and water vapor columns.

3.4.1 Chemistry based validations

McMillan et al [this issue] use DC-8 coincident CO data to provide crucial assessment of AIRS mid-tropospheric CO retrievals (400-500 hPa). Convolution of the in situ profiles with AIRS verticality functions demonstrate AIRS 400-500 hPa CO retrievals are biased high by approximately 8 (± 5)%. Emmons et al., [this issue] use INTEX-A and other available measurements of CO designed to be coincident with MOPITT overpasses for the continued validation of the CO retrievals from the MOPITT instrument onboard the Terra satellite. On average, it is estimated that MOPITT is 7-14% high at 700 hPa and ~3% high at 350 hPa. These results are consistent with previous validation results and are generally within the MOPITT design criteria of 10% accuracy. Figure 8 shows the agreement between MOPITT and DC-8 based CO columns in the troposphere. MOPITT is shown to be useful at describing CO during several meteorological scenarios involving Alaskan fires, urban plumes and a warm conveyor belt, in the middle to upper troposphere [Kiley et al, this issue, 2006b].

Heckel et al. [this issue] and Martin et al. [2006] compare coincident airborne in situ measurements of NO_2 from INTEX-A with those derived from SCIAMACHY. A reasonable correlation is indicated although random errors of the order of 50% are possible [Figure 8]. Martin et al. [2006] further analyze SCIAMACHY and airborne NO_2 data to derive top-down emission estimates via inverse modeling using GEOS-Chem. Their emission inventory for land surface NO_x emissions (46 Tg N yr^{-1}) is 22% larger than the GEIA-based bottom-up inventory for 1998 but is shown to improve the GEOS-Chem simulation of NO_x, PAN, and HNO_3 over eastern NA. Although Aura satellite was launched in July 2004 and not ready for validation during INTEX-A, ozone-CO correlations observed in INTEX-A were compared to summer 2005 correlations observed

by the Aura TES instrument in North American outflow as a test of the ability of TES to observe these correlations [Zhang, et al., 2006].

Millet et al. [this issue] perform a detailed error analysis to conclude that that satellite retrievals of HCHO columns from GOME (and OMI) can be used reliably as a proxy for isoprene emissions over North America. They use aircraft data collected over NA and the Atlantic during INTEX-A and the GEOS-Chem model to draw conclusions about space-based mapping of VOC emissions. From observed HCHO and isoprene profiles they find an HCHO molar yield from isoprene oxidation of 1.6 ± 0.5, consistent with current chemical mechanisms. Retrieval errors, combined with uncertainties in the HCHO yield from isoprene oxidation, result in a 40% (1σ) error in inferring isoprene emissions from HCHO satellite measurements.

3.4.2 Optical property based validations

Russell et al. [this issue] report J-31 AOD measurements using AATS and compare them to retrievals by three satellite sensors: MISR on Terra and MODIS on both Terra and Aqua. Comparisons of MISR and AATS on days with strong AOD gradients over the Gulf of Maine showed that MISR (Versions 15 and 16) nicely captured the AATS-measured AOD gradient (R^2=0.9) for all 4 MISR wavelengths (446 to 866 nm). Comparisons of MODIS and AATS AOD values on 8 overpasses using 61 grid cells yielded R^2=0.97 and RMS difference 0.03, with about 87% of the MODIS AOD retrievals agreeing with AATS values within the MODIS over-ocean uncertainty. In contrast the MODIS-AATS differences in Ångstrom exponent (-dlnAOD/dlnλ) were rather large but improved substantially when cases with small AOD (<0.1 at 855 nm)

were excluded. Water vapor measurements from AATS were in good agreement with those of the in situ Vaisala HMP243 sensor and sondes [Livingston et al., this issue]. However, MODIS infrared retrievals of column water vapor were poorly correlated with ($R^2 = 0.20$) and significantly exceeded those of AATS. In comparison, AIRS layer water vapor agreed with AATS and Vaisala to within 10%.

Kondragunta et al. [this issue] determined that operational GOES AOD imagery provided accurate spatial extent of pollution plumes despite residual cloud contamination in certain pixels. Although the GOES-suborbital AOD differences are notably larger than MODIS-suborbital differences reported by Russell et al. [this issue] and others, Kondragunta et al. [this issue] argue that that GOES AODs are a good proxy to monitor pollution associated with urban/industrial sources and biomass burning events. Results from these INTEX-A validation studies are helping to quantify the tradeoffs between the greater frequency of GOES retrievals from a geostationary, operational satellite and the greater accuracy of more modern sensors on polar orbiting satellites, such as MODIS and MISR.

Pilewskie et al. [this issue] report cloud properties derived from J-31 measurements of visible and near-infrared reflectance in the presence of aerosols. By combining airborne sunphotometer and spectral irradiance data they find that, when an aerosol layer with optical depth >0.1 was present above a cloud, both satellite measurements and spectral irradiances from above the aerosol layer obtained cloud optical depth values less than those obtained from airborne radiometry between the aerosol and cloud layers. Their findings emphasize the importance of quantifying potential biases of retrieved cloud parameters in the presence of aerosol which could be

mistakenly interpreted as an indirect aerosol forcing.

Howell et al. (this issue) looked into apparent disagreements between in-situ and satellite (MISR) measurements of AOD at scales of a few tens of kilometers for a MISR closure flight. While the MISR aerosol retrieval algorithm adequately captured the fundamental two layered aerosol plume (biomass aerosol aloft and pollution below), the retrieved AOD was apparently inconsistent with in-situ aerosol and radiation profiles.

4.0 Conclusion

The INTEX-A/ICARTT measurements provide a rich data set for describing the composition and chemistry of the NA troposphere, for investigating the transformation of gases and aerosols during long-range transport, for the radiation balance of the troposphere, and for validating a variety of satellite observations models of chemistry and transport. The results presented in this special section of JGR represent only the initial analysis and much more integrated analysis is expected in the near future. The data are available to all interested parties for further analysis.

Acknowledgement: We thank all ICARTT participants and sponsoring agencies for making this project possible. DC-8 activities were supported by the NASA Tropospheric Chemistry Program. J-31 activities received partial support from NASA's Radiation Science and NOAA's Atmospheric Composition and Climate Programs. We very much appreciate the dedicated efforts of all DC-8 personnel from NASA Dryden, NASA Wallops, Univ. of North Dakota, and J-31 personnel from Sky Research in make this campaign a success.

References:

Al-Saadi, J., et al., Lagrangian Characterization of the Sources and Chemical Transformation of Air Influencing the Continental US During the 2004 ICARTT/INTEX-A Campaign, J. Geophys. Res., this issue.

Bertram, T.H., et al., Convection and the Age of Air in the Upper Troposphere, J. Geophys. Res., this issue.

Borrell. P., P. M. Borrell, J. P. Burrows, and U. Platt (Eds.), Sounding the troposphere from space: A new era for atmospheric chemistry, pp. 1-446, Springer-Verlag, Berlin, 2004.

Chai, T., G. Carmichael, Y. Tang, et al., Evaluating and improving regional emission estimates using the ICARTT observations, J. Geophys. Res., this issue.

Chatfield, R. B. et al., Intensity of smog ozone production and distribution over eastern North America during ICARTT and a remarkable production-of-ozone estimator, J. Geophys. Res., this issue.

Choi Y. et al. Regional-scale characterization of summertime atmospheric CO_2 variations over the contiguous United States during INTEX-NA, J. Geophys. Res., this issue.

Clarke, A. D., V. Kapustin, S. G. Howell1, C. S. McNaughton1, Y. Shinozuka, B. Anderson, Jack Dibb, Biomass Burning and Pollution Aerosol over North America: Organic Components and their influence on Spectral Optical Properties and Humidification Response, J. Geophys. Res., this issue.

Cook, P. et al., Forest fire plumes over the North Atlantic: p-TOMCAT model simulations with aircraft and satellite measurements from the ITOP/ICARTT Campaign, J. Geophys. Res., this issue.

Cooper, O. R., et al., Large upper tropospheric ozone enhancements above mid-latitude North America during summer: In situ evidence from the IONS and MOZAIC ozone monitoring network, J. Geophys. Res., this issue.

Crawford, J. H., et al., Assessment of upper tropospheric HOx sources over the tropical Pacific based on NASA GTE/PEM data: Net effect on HO_x and other photochemical parameters, J. Geophys. Res., 104, 16,255–16,273, 1999.

Crawford, J., et al., Summertime ozone production over North America during INTEX-A based on observed and modelled photochemistry, J. Geophys. Res., this issue.

Crounse, J. D., K. A. McKinney, A. J. Kwan, and P. O. Wennberg, Measurement of gas-phase hydroperoxides by chemical ionization mass spectrometry (CIMS), Anal. Chem., in press, 2006a.

Crounse, J., P. O. Wennberg, A. J. Kwan, B. Heikes, O'Sullivan, Shen, J. Crawford, Peroxyacetic acid is ubiquitous in the upper troposphere, Geophys. Res. Lett., submitted, 2006b.

Day, D. A., P. J. Wooldridge, M. B. Dillon, J. A. Thornton, and R. C. Cohen, A thermal dissociation laser-induced fluorescence instrument for in situ detection of NO_2, peroxy nitrates, alkyl nitrates, and HNO_3, J. Geophys. Res., 107(D6), 4046, doi:10.1029/2001JD000779, 2002.

Derwent, R. G. et al., External influences on Europe's air quality: Baseline methane, carbon mo**NO_x**ide and ozone from 1990 to 2030 at Mace Head, Ireland, Atmos. Environ., 40(5), 844-855, 2006.

Dibb, J. E., E. Scheuer, R. Talbot, M. Avery, T. Bertram, R, Cohen, Stratospheric Influence on the Composition of the Mid- and Upper-Troposphere over North America sampled by the NASA DC-8 during INTEX A, J. Geophys. Res., this issue.

Emmons, L. K., G. G. Pfister, D. P. Edwards, J. C. Gille, G. Sachse, D. Blake, S. Wofsy, C. Gerbig, D. Matross, P. Nédélec, MOPITT validation exercises during Summer 2004 field campaigns over North America, J. Geophys. Res., this issue.

Fehsenfeld, F. C.; M. Trainer, M.; D. D. Parrish, A. Volz-Thomas; S. Penkett, North Atlantic Regional Experiment 1993 summer intensive: Foreword, J. Geophys. Res. Vol. 101 (D22), 28,869-28,875, 1996

Fehsenfeld, F. C. et al., International Consortium for Atmospheric Research on Transport and Transformation (ICARTT): North America to Europe: Overview of the 20004 summer study, J. Geophys. Res., submitted, 2006.

Fried, A., et al., The Role of Convection in Redistributing Formaldehyde to the Upper Troposphere over North America and the North Atlantic during the Summer 2004 INTEX Campaign, J. Geophys. Res., this issue.

Fuelberg, H. E., M. J. Porter, C. M. Kiley, D. Morse, Meteorological conditions and anomalies During INTEX-NA, J. Geophys. Res., this issue.

Grousset, F.E., P. Ginoux, A, Bory, P. E. Biscaye, Case study of a Chinese dust plume reaching the French Alps, Geophys Res. Letts., 30(6), 10-1, 2003.

Guerova, G., I. Bey, J.-L. Atti´e, R. V. Martin, J. Cui, and M. Sprenger, Impact of transatlantic transport episodes on summertime ozone in Europe, Atmos. Chem. Phys., 6, 2057–2072, 2006.

Heckel, A., et al., Validation of SCIAMACHY tropospheric NO_2 and HCHO columns during INTEX-A/ICARTT, J. Geophys. Res., this issue.

Hoell, J. M., D. D. Davis, S. C. Liu, R. Newell, M. Shipham, H. Akimoto, R. J. McNeal, R. J. Bendura, and J. W. Drewry, Pacific Exploratory Mission-West A (PEM-West A): September–October 1991, J. Geophys. Res., 101, 1641– 1653, 1996.

Hoell, J. M., D. D. Davis, S. C. Liu, R. E. Newell, H. Akimoto, R. J. McNeal, and R. J. Bendura, The Pacific Exploratory Mission-West Phase B: February–March, 1994, J. Geophys. Res., 102, 28,223– 28,239, 1997.

Holloway, T., A. M. Fiore, M. G. Hastings, Intercontinental Transport of Air Pollution: Will emerging science lead to a new hemispheric treaty?, Environ. Sci. & Technol, 37, 4535-4542, 2003.

Horowitz, L. W., et al., A global simulation of tropospheric ozone and related tracers: description and evaluation of MOZART, version 2, J. Geophys. Res, 108 (D24), 4784, doi:10.1029/2002JD002853, 2003.

Horowitz, L. W., A. M. Fiore, G. Milly, R. C. Cohen, A. Perring, and P. J. Woolridge, Observational constraints on the chemistry of isoprene nitrates over the eastern United States, J. Geophys. Res., this issue

Howell, S. C. et al., Satellite Aerosol Optical Depth Measurements in a Complex Environment: A Case Study Comparing Aircraft and Ship Measurements With MISR During INTEX-NA, J. Geophys. Res., this issue.

Houghton, J. T. et al., IPCC Climate Change 2001: The Scientific Basis, Cambridge Univ. Press, New York, 2001.

Hudman R.C., et al., A multi-platform analysis of the North American reactive nitrogen budget during the ICARTT summer intensive, J. Geophys. Res., this issue.

Huey, L. G., et al., Measurement of HO_2NO_2 in the Upper Troposphere during INTEX-NA 2004, J. Geophys. Res., this issue.

Huntrieser, J., et al., Intercontinental air pollution transport from North America to Europe: Experimental evidence from airborne measurements and surface observations, J. Geophys. Res., 110(D01), 305, doi:10.1029/2004JD005045, 2005.

Jacob, D. J., Logan, J., and Murti, P.: Effect of rising Asian emissions on surface ozone in the United States, Geophys. Res. Lett., 26, 2175–2178, 1999.

Jacob, D. J., J. H. Crawford, M. M. Kleb, V. S. Connors, R. J. Bendura, J. L. Raper, G. W. Sachse, J. C. Gille, L. Emmons, and C. L. Heald, Transport and Chemical Evolution over the Pacific (TRACE-P) aircraft mission: Design, execution, and first results, J. Geophys. Res., 108(D20), 9000, doi:10.1029/2002JD003276, 2003.

Jaffe, D., et al., Transport of Asian air pollution to North America, Geophys. Res. Lett., 26(6*),* 711–714, 1999.

Jaffe, D., H. Price, D. Parrish, A. Goldstein, and J. Harris, Increasing background ozone during spring on the west coast of North America, Geophys. Res. Lett., 30(12), 1613, doi:10.1029/2003GL017024, 2003.

Kiley, C. M. and H. E. Fuelberg, An examination of summertime cyclone transport processes during INTEX-A, J. Geophys. Res., this issue, 2006a.

Kiley, C. M., H. E. Fuelberg, L. Emmons, J. Gille, D. Mao, Y. Tang, G. Carmichael, An investigation of warm season co transport episodes during intex-a using synthetic mopitt imagery, J. Geophys. Res, this issue, 2006b.

Kondragunta, S., P. Ciren, A. I. Prados, Y. Shinozuka, A. Clarke, Characterization of GOES-12 Aerosol Optical Depth Retrievals during ICARTT/INTEX-A, J. Geophys. Res, this issue.

Kahn, R., A. Clarke, S. Howell, J. Livingston, C. McNaughton, P. Quinn, J. Redemann, P. Russell, B. Schmid, M. Bull, D. Nelson, Aerosol Properties from MISR Space-based Multi-angle Imaging: INTEX-NA Campaign Validation and Results. J. Geophys. Res., this issue.

Kwan, A. J., John D. Crounse, A. D. Clarke, Y. Shinozuka, B. E. Anderson, J. H. Crawford, M. A. Avery, C. S. McNaughton, W. H. Brune, H. B. Singh, and P. O. Wennberg, On the flux of oxygenated volatile organic compounds from organic 3 aerosol oxidation, Geophys. Res. Lett.*,* in press, 2006.

Law, K. et al., Evidence for Long-Range Transport of North American Anthropogenic and Wildfire Emissions to Europe from Airborne and Ground Based Lidar Measurements during European ITOP (IGAC Lagrangian 2K4, ICARTT), Fall AGU, A41D-01, 2005.

Lelieveld, J. et al., Global Air Pollution Crossroads over the Mediterranean, Science, 298, 794-799, 2002.

Liang, Q. et al., Summertime influence of Asian pollution in the free troposphere over North America, J. Geophys. Res., this issue.

Livingston, J. et al., Comparison of water vapor measurements by airborne sunphotometer and near-coincident in situ and satellite sensors during INTEX-A 2004, J. Geophys. Res., this issue.

Mena-Carrasco, M. et al., Improving regional ozone modeling through systematic evaluation of errors using the aircraft observations during ICARTT, J. Geophys. Res., this issue.

Martin, R. V., et al., Evaluation of space-based constraints on global nitrogen oxide emissions with regional aircraft measurements over and downwind of eastern North America, J. Geophys. Res, in press, 2006.

McMillan,W. W., et al., AIRS views of transport from 12-22 July 2004 Alaskan/Canadian fires: Correlation of AIRS CO and MODIS AOD with forward trajectories and comparison of AIRS CO retrievals with DC-8 in situ measurements during INTEX-A/ICARTT, J. Geophys. Res, this issue.

Methven, J. et al., Establishing Lagrangian connections between observations within air masses crossing the Atlantic during the ICARTT experiment, J. Geophys. Res, submitted, 2006.

Millet, D. B. et al., Formaldehyde distribution over North America: Implications for satellite retrievals of formaldehyde columns and isoprene emission, J. Geophys. Res, this issue.

Oltmans, S. J. et al., Long-term changes in tropospheric ozone, Atmos. Environ. 40 (17), 3156-3173, 2006.

Parrish, D. D., et al., Changes in the photochemical environment of the temperate North Pacific troposphere in response to increased Asian emissions, J. Geophys. Res., 109, D23S18, doi:10.1029/2004JD004978, 2004.

Penkett, S. A., Volz-Thomas, A., Parrish, D. D., Honrath, R. E., Fehsenfeld, F. C. Preface, J. Geophys. Res. 103 (D11) , 13,353, 1998.

Pilewskie, P., O. Hofmann, B. Kindel, W. Gore, P. Russell, J. Livingston, J. Redemann, R. Bergstrom, S. Platnick, J. Daniel, T. Garrett, Cloud Properties Derived from Visible and Near-infrared Spectral Albedo in the Presence of Aerosols, J. Geophys. Res., this issue.

Pfister G., P. G. Hess, L. K. Emmons, J.-F. Lamarque, C. Wiedinmyer, D. P. Edwards, G. Pétron, J. C. Gille, G. W. Sachse, Quantifying CO emissions from the 2004 Alaskan wildfires using MOPITT CO data, Geophys. Res. Lett., 32, L11809, doi:10.1029/2005GL022995, 2005.

Pfister, G. et al., Ozone Production from Boreal Forest Fire Emissions, J. Geophys. Res., this issue.

Pierce, R. B. et al., Regional Air Quality Modeling System (RAQMS) predictions of the tropospheric ozone budget over east Asia, J. Geophys. Res, 108, D21, 8825, doi:10.1029/2002JD003176, 2003.

Pierce, R. B., et al., Chemical data assimilation based estimates of Continental US Ozone and Nitrogen budgets during INTEX-A, J. Geophys. Res., this issue.

Porter, M., H. et al., Assesing convective influence by utilizing cloud to ground lightning data and high resolution kinematic trajectories, J. Geophys. Res., this issue.

Raper, J. L., M. M. Kleb, D. J. Jacob, D. D. Davis, R. E. Newell, H. E. Fuelberg, R. J. Bendura, J. M. Hoell, and R. J. McNeal, Pacific Exploratory Mission in the tropical Pacific: PEM-Tropics B, March–April 1999, J. Geophys. Res., 106, 32,401–32,425, 2001.

Redemann, J. et al. Airborne measurements of spectral direct aerosol radiative forcing in the Intercontinental chemical Transport Experiment/Intercontinental Transport

and Chemical Transformation of anthropogenic pollution, 2004, J. Geophys. Res., 111, No. D14, D14210 10.1029/2005JD006812, 26 July 2006.

Ren, X., et al., HO_x observation and model comparison during INTEX-NA 2004, J. Geophys. Res., this issue.

Richter, A. J. P. Burrows, H. Nü, C. Granier, U. Niemeier, Increase in tropospheric nitrogen dioxide over China observed from space, Nature, 437, 129-132, 2005.

Russell, P. B., P. V. Hobbs, L. L. Stowe, Aerosol properties and radiative effects in the United States East Coast haze plume: An overview of the Tropospheric Aerosol Radiative Forcing Observational Experiment (TARFOX), J. Geophys. Res,104 (D2), 2213–2222, 1999.

Russell, P. B. et al., Multi-Grid-Cell validation of satellite aerosol property retrievals in INTEX/ITCT/ICARTT 2004 , J. Geophys. Res., this issue.

Schere, K. L., G. M. Hidy, and H. B. Singh (Eds), The NARSTO Ozone Assessment-critical reviews, Atmos. Environ., 34(12-14), 1853-2332-4778, 2000.

Schoeberl, M. R., et al., Earth observing system missions benefit atmospheric research, EOS, Vol. 85, No. 18, 2004. (http://eos-aura. gsfc.nasa.gov/).

Seinfeld, J. H. and S. N. Pandis, Atmospheric Chemistry and Physics, John Wiley and Sons, New York, 1998.

Shinozuka, Y., A. D. Clarke, S. G. Howell, V, Kapustin, C. S. McNaughton, J. Zhou, Aircraft profiles of aerosol microphysics and optical properties over North America: aerosol optical depth and its association with PM2.5 and water uptake, J. Geophys. Res., this issue.

Simmonds, P. G., R. G. Derwent, A. L. Manning and G. Spain, Significant growth in surface ozone at Mace Head, Ireland, 1987–2003, Atmos. Environ., 38(28), 4769-4778, 2004.

Singh, H. B., A. Thompson, and H. Schlager, SONEX airborne mission and coordinated POLINAT-2 activity: overview and accomplishments, Geophys. Res. Lett., 26, 3053-3056, 1999.

Singh, H. B., D. J. Jacob, L. Pfister, J. H. Crawford, INTEX-NA: Intercontinental Chemical Transport Experiment-North America, December 2002. (http://cloud1.arc.nasa.gov).

Singh, H. B., et al., Reactive Nitrogen Distribution and Partitioning in the North American Troposphere and Lowermost Stratosphere, J. Geophys. Res., this issue.

Snow, J., B. Heikes, D. O'Sullivan, E. Shen, A. Fried, and Wallega, Hydrogen peroxide and methylhydroperoxide mixing ratios over North America and the North Atlantic during INTEX-NA. J. Geophys. Res., this issue.

Stohl, A. and Trickl, T., A textbook example of long-range transport: Simultaneous observation of ozone maxima of stratospheric and North American origin in the free troposphere over Europe, J. Geophys. Res., 104, 30 445–30 462, 1999.

Stohl, A. (Ed.). Intercontinental transport of Air Pollution, The Handbook of Environmental Chemistry, Springer-Verlag, Berlin, pp. 320, 2004.

Tang, Y., et al., Three-dimensional simulations of inorganic aerosol distributions in East Asia during spring 2001, J. Geophys. Res., 109, D19S23, doi:10.1029/2003JD004201, 2004.

Tarasick, D. W., et al., Comparison of Canadian Air Quality Forecast Models With Tropospheric Ozone Profile Measurements Above Mid-Latitude North America

During the IONS/ICARTT Campaign: Evidence for Stratospheric Input, J. Geophys. Res., this issue.
Thompson, A. M. et al., IONS (INTEX Ozonesonde Network Study, 2004). 1. Perspective on Summertime UT/LS (Upper Troposphere/Lower Stratosphere) Ozone over Northeastern North America, J. Geophys. Res., 2006JD007441, this issu, 2006a.
Thompson, A. M. et al., IONS-04 (INTEX Ozonesonde Network Study, 2004). 2. Tropospheric Ozone Budgets and Variability over Northeastern North America, J. Geophys. Res., doi: 10.129/2006JD007670, this issue, 2006b.
Turquety, S., et al., Inventory of boreal fire emissions for North America: importance of peat burning and pyro-convective injection, J. Geophys. Res., this issue.
VanCuren, R. A., Asian aerosols in North America: Extracting the chemical composition and mass concentration of the Asian continental aerosol plume from long term aerosol records in the western United States, J. Geophys. Res., 108(D20), 4623, doi:10.1029/2003JD003459, 2003.
Vadrevu, K. et al. Linking Airborne Measurements of **CO_2** with Terrestrial Sources of Carbon over Heterogenous Landscapes, J. Geophys. Res., this issue.
Vingarzan, R. A review of surface ozone background levels and trends, Atmos. Environ., 38(21), 3431-3442, 2004.
Washenfelder, R. A., G. C. Toon, J-F. Blavier, Z. Yang, N. T. Allen, P. O. Wennberg, S. A. Vay, D. M. Matross , B. C. Daube, Carbon dioxide column abundances at the Wisconsin Tall Tower site, J. Geophys. Res., in press, 2006.
Yu, S., R. Mathur, K. Schere, D. Kang, J. Pleim, and T. L. Otte, A comprehensive evaluation of the Eta-CMAQ forecast model performance for O_3, its related precursors, and meteorological parameters during the 2004 ICARTT study, J. Geophys. Res., this issue.
Zhang, L., et al., Continental outflow of ozone pollution as determined by O_3-CO correlations from the TES satellite instrument, submitted to Geophys. Res. Lett, 2006.

Appendix A: A list of Acronyms

AATS: Ames Airborne Tracking Sunphotometer
AERONET: Aerosol Robotic Network
AIRS: Atmospheric Infrared Sounder
AOD: Aerosol Optical depth
AURAMS: A Unified Regional Air-quality Modelling System
AVHRR: Advanced Very High Resolution Radiometer
CHRONOS: Canadian Hemispheric and Regional Ozone and **NO_x** System
CIMS: Chemical Ionization Mass Spectrometry
CMAQ: Community Multiscale Air Quality
CTM: Chemical Transport Model
DLR: Deutschen Zentrum für Luft- und Raumfahrt
GOES: Geostationary Operational Environmental Satellite
ICARTT: International Consortium for Atmospheric Research on Transport and Transformation

INTEX-NA: Intercontinental Chemical Transport Experiment-North America
IONS: INTEX Ozonesonde Network Study
ITCT: Intercontinental Transport and Chemical Transformation
LIS: Lightning Imaging Sensor
MISR: Multiangle Imaging SpectroRadiometer
MOPITT: Measurement of Pollution in the Troposphere
MOZAIC: Measurement of Ozone on Airbus In-service Aircraft
MOZART: Model of Ozone and Related Tracers
MODIS: Moderate Resolution Imaging Spectroradiometer
NA: North America
NCEP: National Centers for Environmental Prediction
NOAA: National Oceanic and Atmospheric Administration
NASA: National Aeronautics and Space Administration
OC: Organic Carbon
OMI: Ozone Monitoring Instrument
OVOC: Oxygenated Volatile Organic Chemicals
RAQMS: Real-time Air Quality Modeling System
SCIAMACHY: Scanning Imaging Absorption Spectrometer for Atmospheric Chartography
SSFR: Solar Spectral Flux Radiometer
STEM: Sulfur Transport and Deposition Model
TES: Tropospheric Emission Spectrometer
TOMCAT: Toulouse Offline Model of Chemistry and Transport
TOMS: Total Ozone Measuring Spectrometer
UT: Upper Troposphere

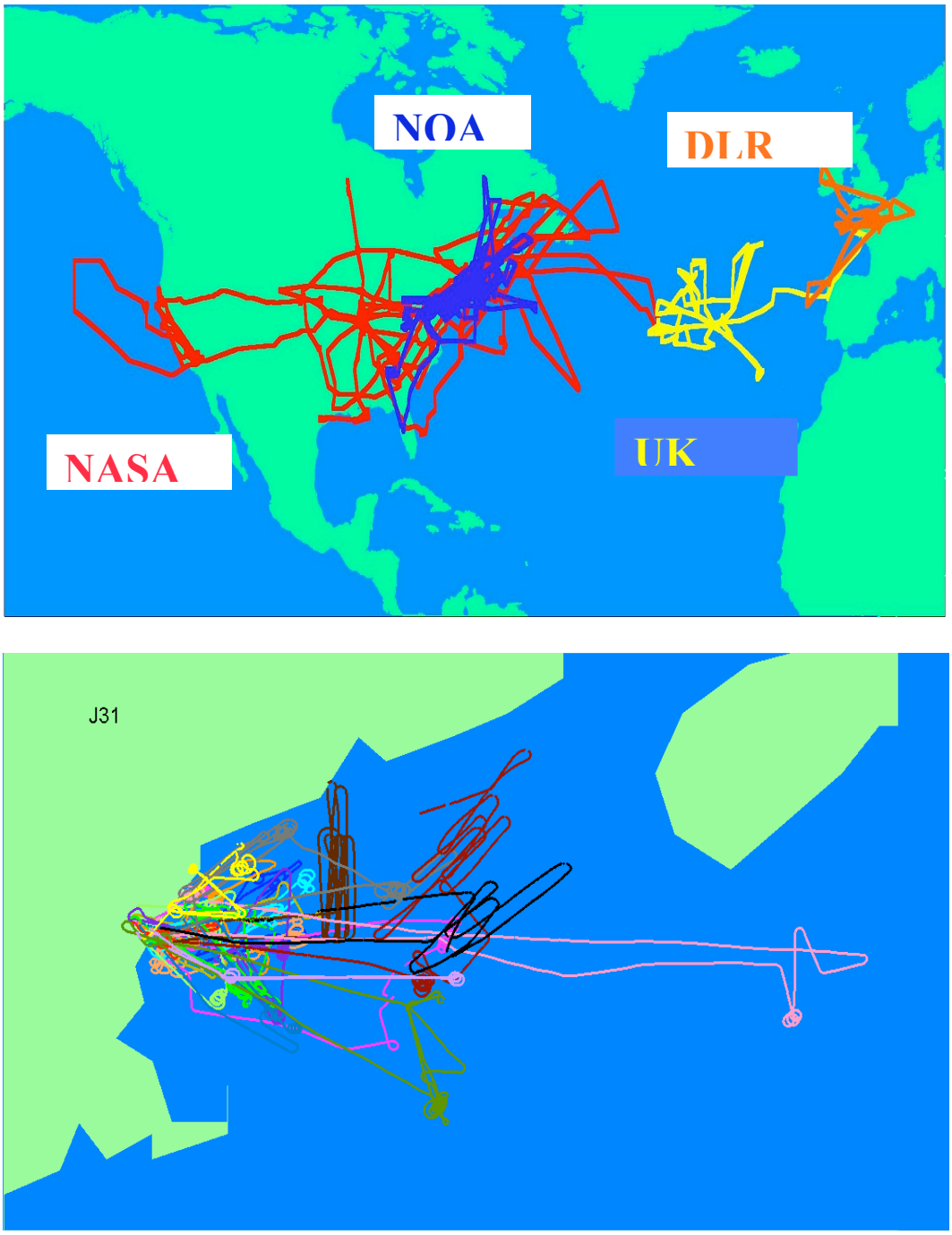

Figure 1: INTEX-ICARTT Flight Tracks of multiple platforms studying air chemistry (top); and radiation (bottom). The top figure is bounded by Lat: 10-70˚N; Long. 150˚W -15˚E and the bottom by Lat: 41-45 ˚N; Long. 290-296˚W.

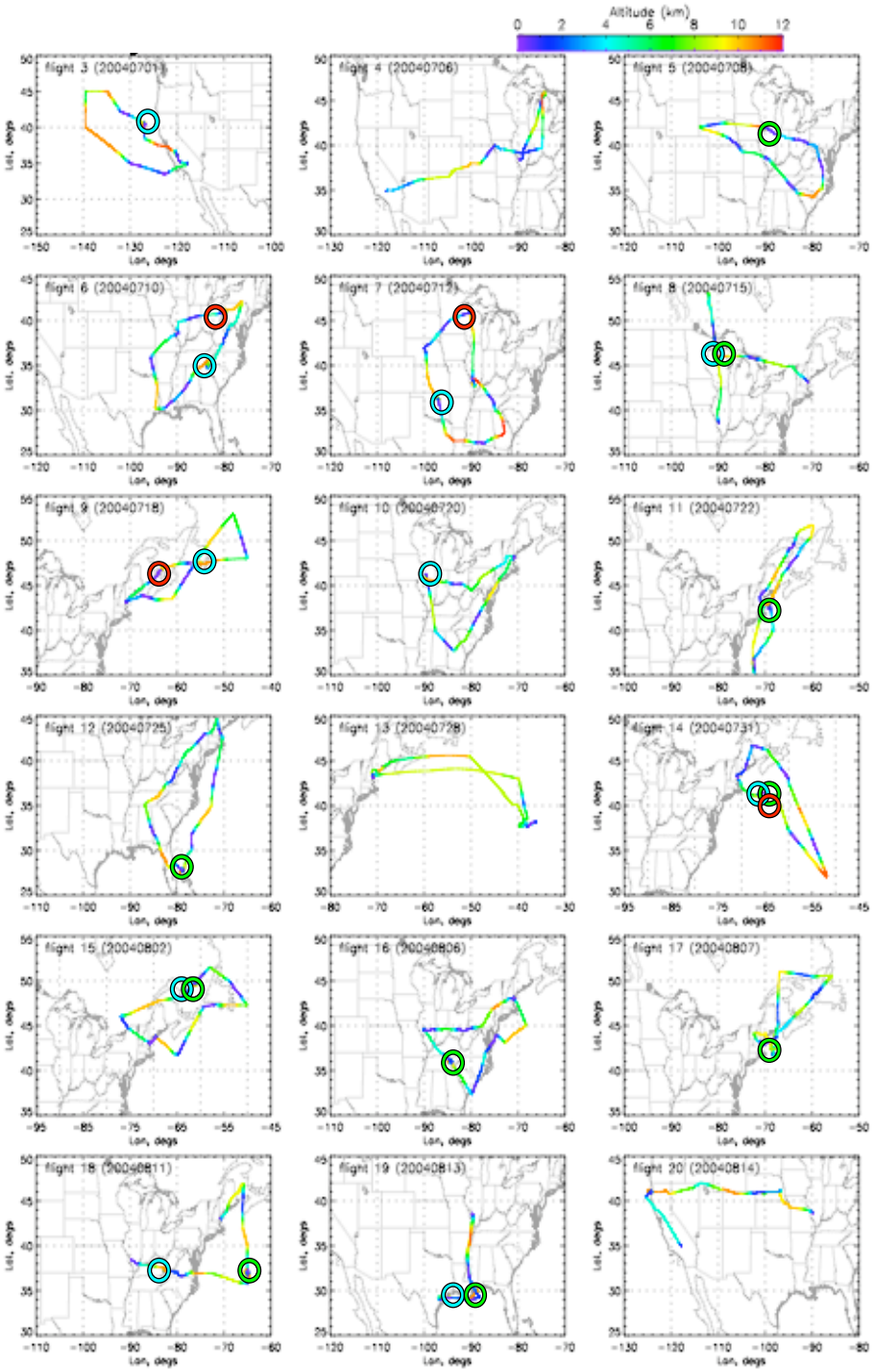

Figure 2: DC-8 flight tracks during INTEX-A. Circles indicate spirals designed for satellite validation for Aqua (blue), Terra (green), and Envisat (red)

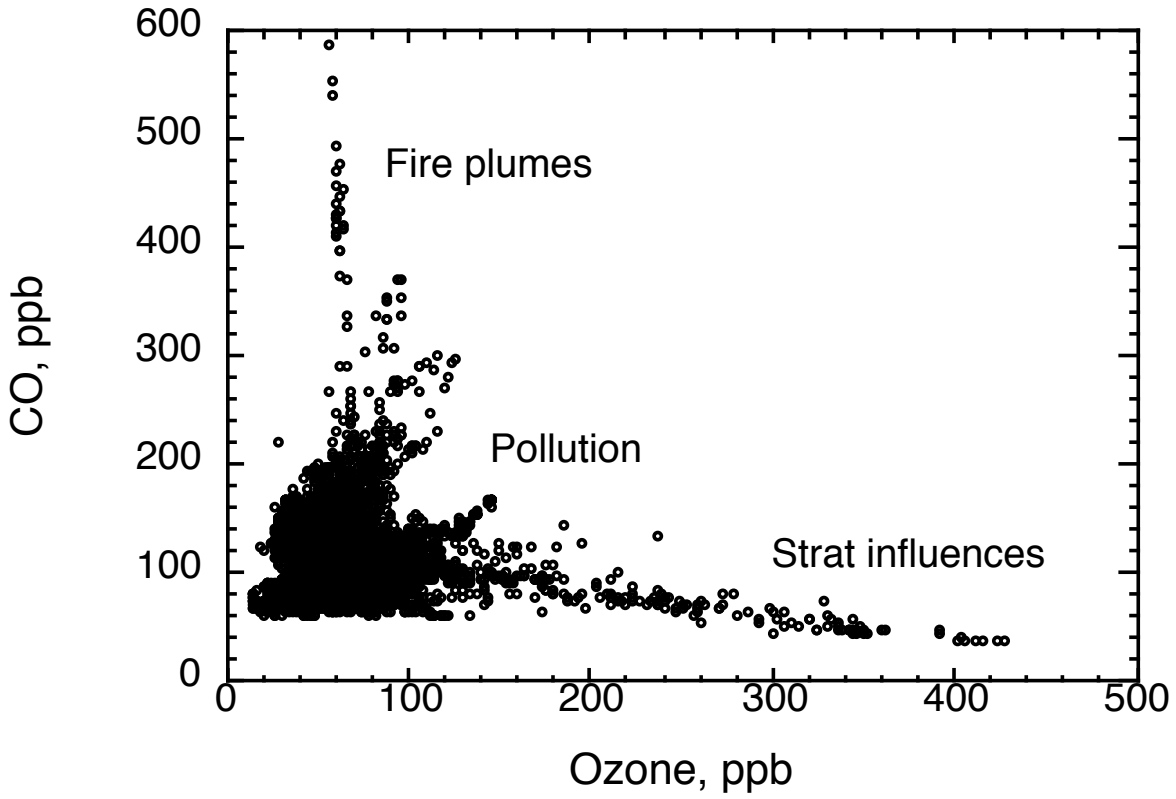

Figure 3: Fire plumes, anthropogenic pollution, and stratospheric influences sampled during INTEX-A

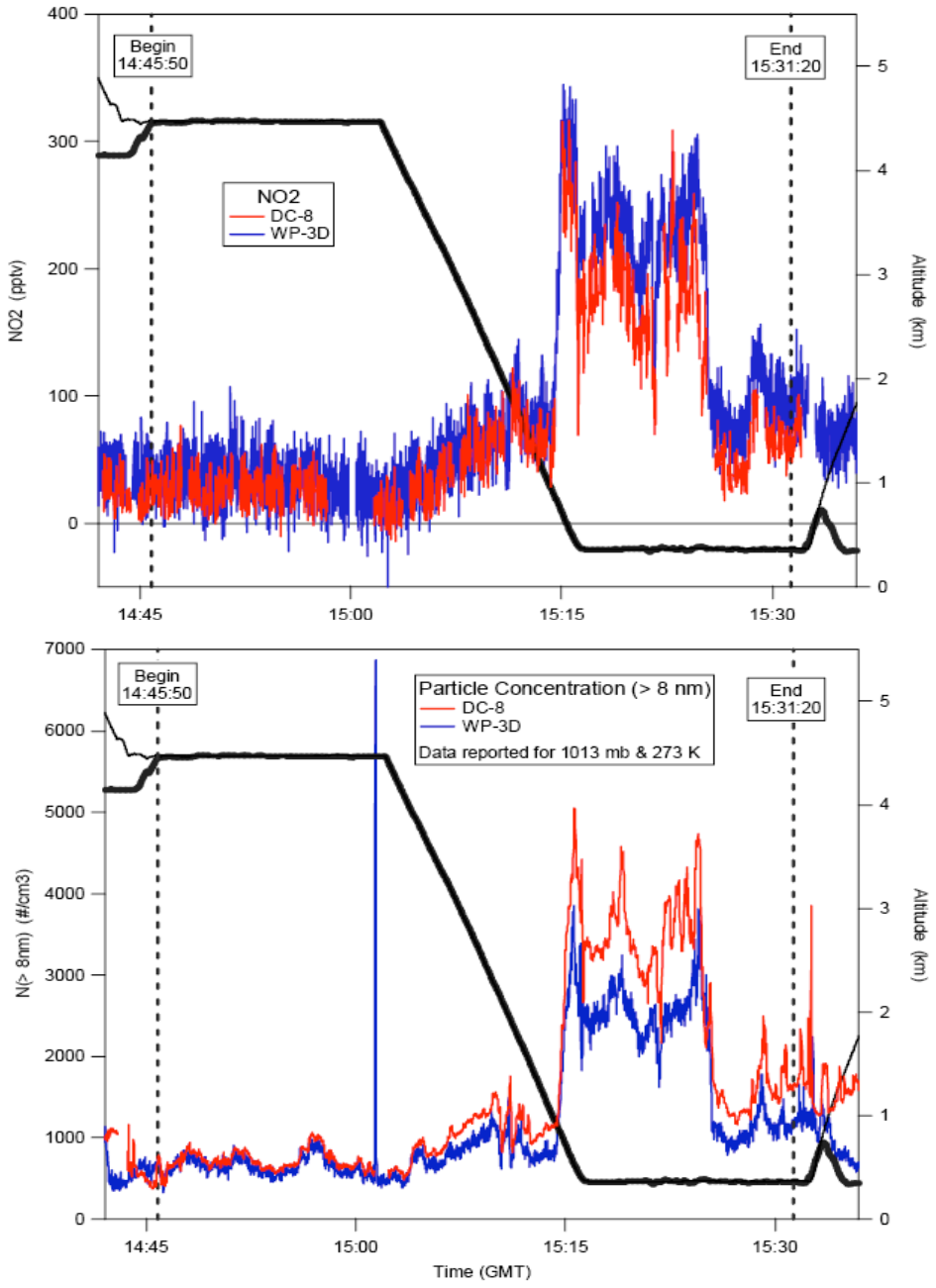

Figure 4: Wingtip to wingtip Inter-comparison flight on July 22, 2004- An example showing measurement of NO_2 (top) and particle count (> 8 nM) on the NASA DC-8 (red) and the NOAAWP-3D (blue).

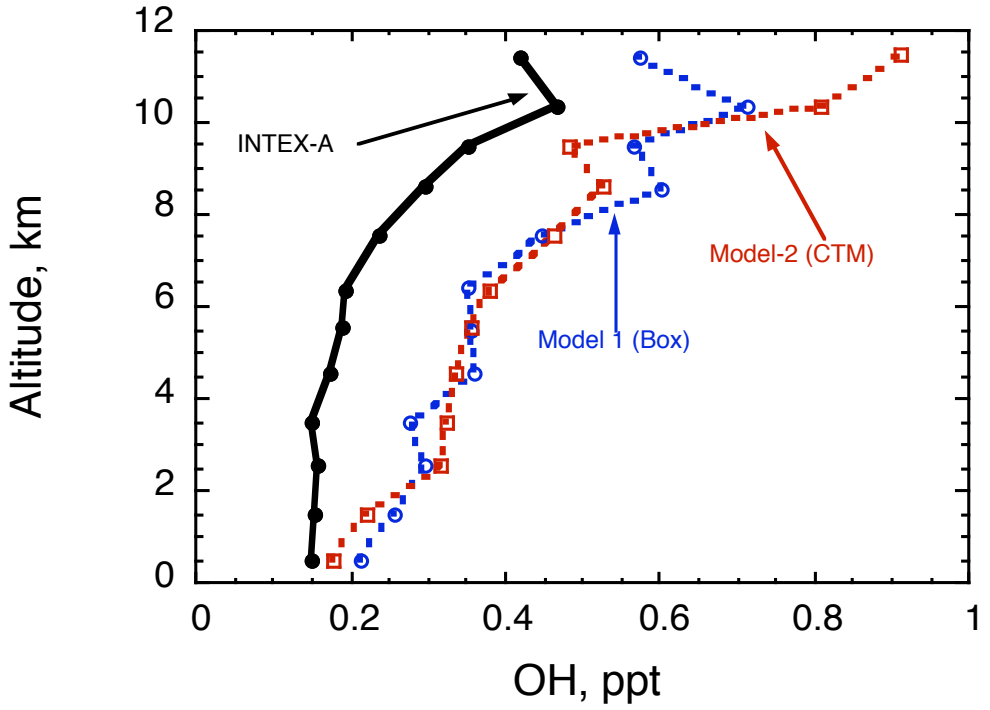

Figure 5: Observed and modeled OH mixing ratios in INTEX-A

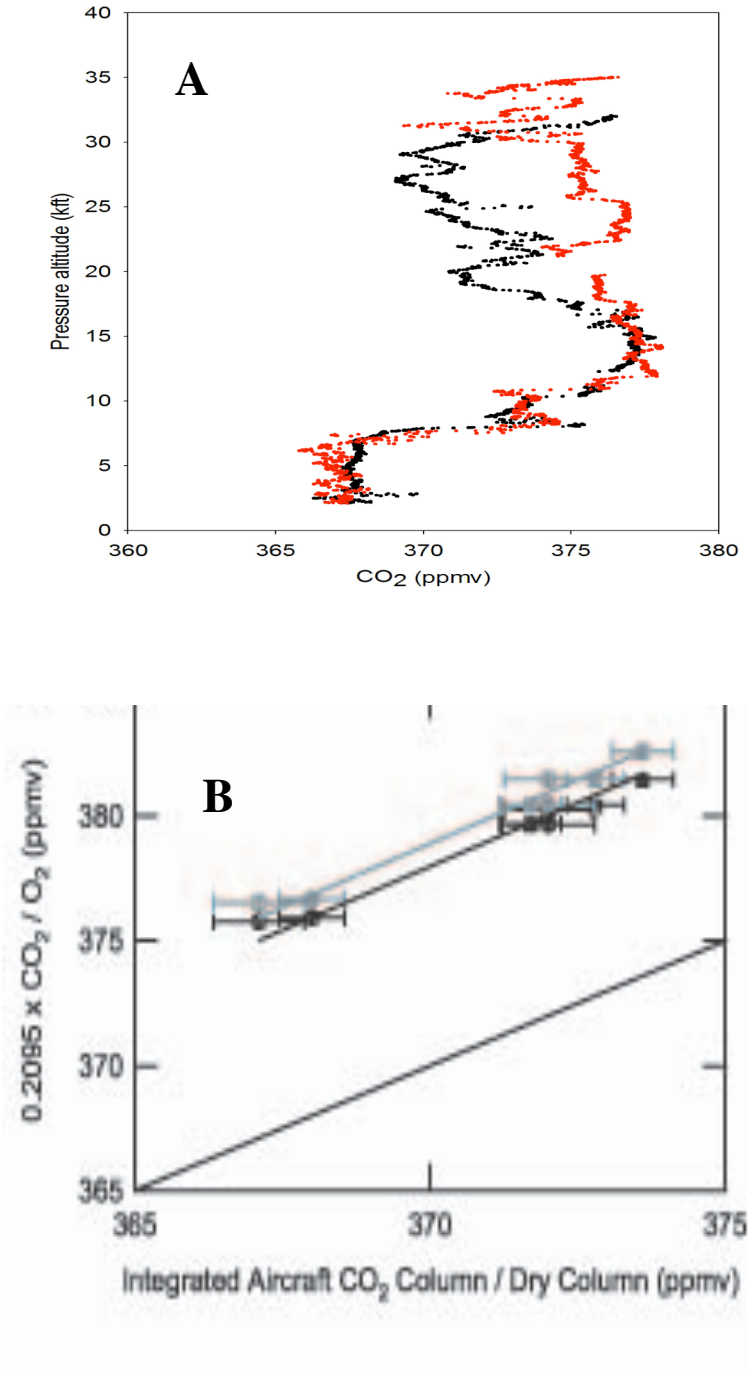

Figure 6: In situ and column CO_2 measurements during INTEX-A at the Wisconsin WLEF Tall Tower site. (A) vertical structure of CO_2 and short-term variability; (B) FTS column measurement comparison with in situ CO_2 columns using two CO_2 bands

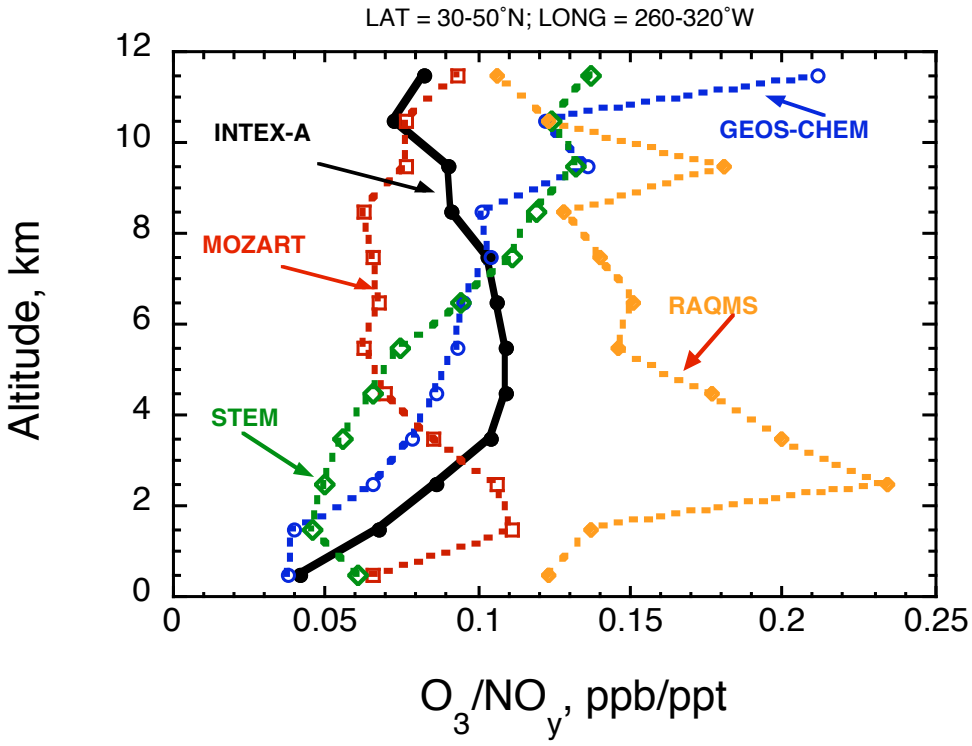

Figure 7: A comparison of observed and simulated O_3/NO_y ratios indicating uncertainties among four selected models

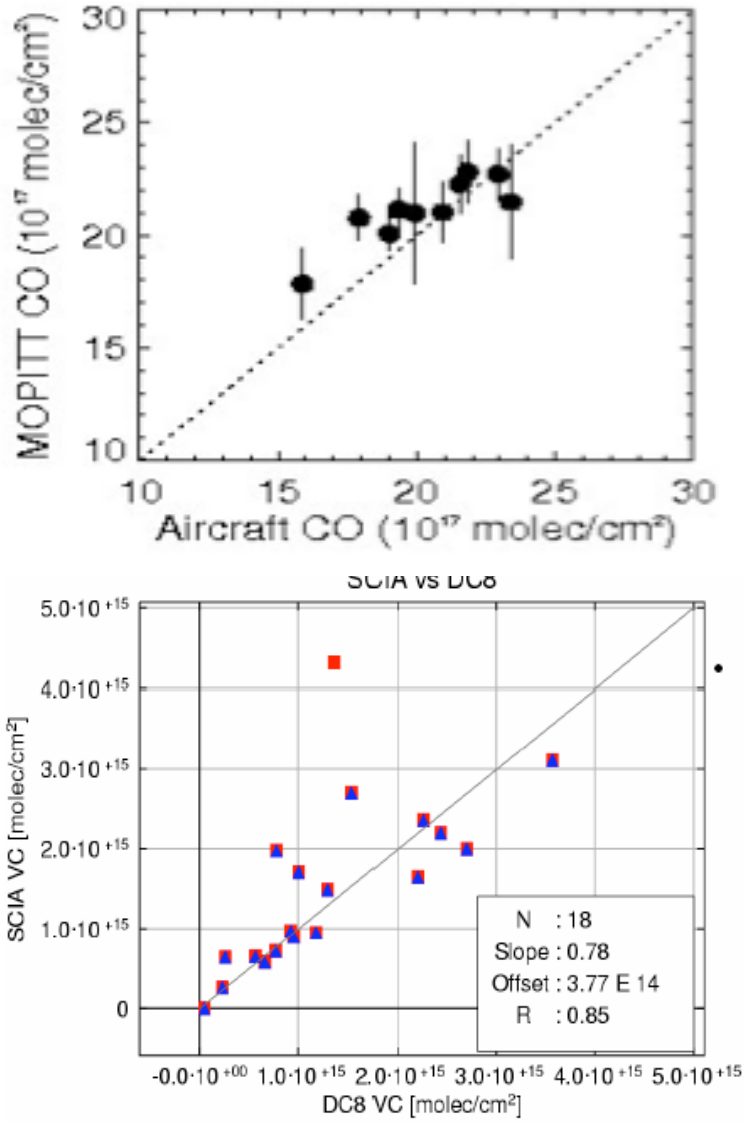

Figure 8: Comparison of MOPITT CO (A) and SCIMACHY NO_2 (B) tropospheric column retrievals with the INTEX-A DC8 in situ profiles transformed by the corresponding averaging kernels.

Table 1: Principal mobile platforms in operation during the summer 2004 ICARTT study

Platform type	Study name	Platforms (*Country*)	Dates of operation (2004)	Bases of operation[$]	Nominal Specifications (km)	
					Altitude	Range
Airborne	INTEX-A	NASA DC-8** (*U. S.*)	7/1-8/15	DR, MA, PT	0.2-12.5	9000
	INTEX-A	NASA/Sky Research J-31[##] (*U. S.*)	7/12-8/8	PT	0.1-7.5	1500
	NEAQS-ITCT	NOAA WP-3D** (*U. S.*)	7/1-8/15	PT	0.1-7.5	6000
	NEAQS-ITCT	NOAA DC-3** *(U. S.)*	7/1-8/15	PT	0.1-3.6	1500
	NEAX	DOE G-1**(*U. S.*)	7/19-8/15	LT	0.3-7.5	2000
	AIF	CIRPAS Twin Otter[##] (*U. S.)*	8/2-8/20	CL	0.1-3.1	500
	ITOP	NERC BAe146-300**(*U. K.*)	7/12-8/4	AZ	0.1-10.5	2000
	ITOP	DLR Falcon-20** (*Germany*)	7/5-8/6	OB, CR	0.1-12.8	3500
	CTC-TIMS	NRC-IAR Convair 580[##] (*Canada*)	7/21-8/18	CL	0.1-7.5	5000
Surface*/ Ship	NEAQS-ITCT	NOAA R/V Ronald H. Brown (*U. S.*)	7/5-8/13	Gulf of Maine	Surface	21000
Space-borne[#]	Terra-NASA	Terra (MOPITT, MISR, MODIS) (*U. S.*)	All year	Space	All altitudes	Global coverage
	Aqua-NASA	Aqua (AIRS, MODIS) (*U. S.*)				
	Envisat-ESA	Envisat (SCIAMACHY) (*E. U.*)				

* A number of fixed surface stations and sonde release sites also operated during this experiment. See Fehsenfeld et al. [2006] for a detailed overview of these.

[#] Principal focus was on chemical measurements in the troposphere

**Extensive payload principally designed to study atmospheric composition and chemistry. DC-8 & DC-3 also contained ozone/aerosol lidar.

[##] J-31 payload (see text) was principally designed to study aerosols and radiation and Convair & Twin Otter to study aerosols and clouds.

[$] DR: Dryden Flight Research Center, CA (34.9˚N, 117.9˚W); MA: Mid-America/Mascoutah, IL (38.5˚N, 89.8˚W); PT: Pease International Tradeport, NH (43.1˚N, 70.8˚W); LT: Latrobe, PA (40.3˚N, 79.4˚W); CL: Cleveland, OH (41.3˚N, 81.4˚W); AZ: Azores, Portugal (38.6˚N, 28.7˚W); OB: Oberpfaffenhofen, Germany (48.1˚N, 11.3˚E); CR: Creil, France (49.3˚N, 2.5˚E)

Table 2A: DC-8 Science Payload during INTEX-A*

Parameters	Method	Principal Investigators	Detection limit/response (Nominal accuracy)
O_3	NO/O_3 Chemiluminescence	M. Avery, NASA LaRC	1 ppb/1 s (±5%)
O_3 & aerosol profile	UV DIAL Lidar	E. Browell, NASA LaRC	-/60 s (±10%)
NO NO_2, HCHO	LIF	D. Tan, GIT	5 ppt/60 s (±10%) 15 ppt/60 s (±10%)
NO_2 NO_y	LIF & thermal dissociation	R. Cohen, UC Berkeley	1 ppt/60 s (±10%) 10 ppt/60 s(±10%)
PANs OVOC, nitriles	GC-ECD/PID/RGD	H. Singh, NASA ARC	1 ppt/90s (±15%) 10 ppt/120 s (±20%)
HNO_3, H_2O_2, organic acids	CIMS	P. Wennberg, Cal Tech	5 ppt/10 s (±15%)
H_2O_2, CH_3OOH, HCHO	Derivative HPLC & fluorescence	B. Heikes, U. Rhode Island	20 ppt/150 s (±20%)
HCHO	TDL Absorption Spectrometry	A. Fried, NCAR	20 ppt/60 s (±10%)
OH, HO_2 naphthalene	LIF	W. Brune, Penn State Univ.	0.02 ppt/15 s (±15%) 10 ppt/15 s (±15%)
SO_2, HNO_4	CIMS	G. Huey, GIT	5 ppt/15 s (±15%)
NMHC, halocarbons, alkyl nitrates	Whole air samples; GC-FID/EC/MS	D. Blake, UC Irvine E. Atlas, U. Miami	1 ppt/100 s (±2-10%)
CO, CH_4, N_2O	TDL Absorption spectrometry	G. Sachse, NASA LaRC	1 ppb/5 s (±5%)
CO_2	Non-Dispersive Infrared	S. Vay, NASA LaRC	0.1 ppm/1 s (±0.1%)
H_2O	Open Path TDLr Absorption Spectrometry	G. Diskin, NASA LaRC; J. Podolske, NASA ARC	5 ppm /10 s (±5%)
H_2O $J(NO_2)$	Cryogenic hygrometer, filter radiometer	J. Barrick, NASA LaRC	5 ppm /10 s (±10%) 10^{-6} s /20 s (±10%)
Aerosol bulk ionic composition	Particle Into Liquid Sampling (PILS)/IC	R. Weber, GIT	5 ppt/150 s (±15%)
Bulk aerosol composition, HNO_3	Mist Chamber/IC	R. Talbot, UNH	10 ppt/300 s (±15%)
Aerosol number, size, composition, microphysics, optical properties, light absorption & scattering, cloud water content	Particle Spectrometers, volatility TDMA, CN counters, nephelometer, soot photometer, f(RH), cloud and aerosol probes	A. Clarke, U. Hawaii B. Anderson, NASA LaRC	
Actinic fluxes & photolytic frequencies	Spectral radiometery, Zenith & Nadir	R. Shetter, NCAR	10^{-8} s /15 s (±5%)

Table 2B: J-31 Science Payload during INTEX-A*

Parameters	Method	Principal Investigators	Detection limit/response (Nominal accuracy)
Optical depth, water vapor column	Tracking Sun photometer, 354-2138 nm	P. Russell, NASA ARC	Slant OD ~0.002/3 s (±0.01) Slant WV ~0.0005 to 0.006 cm^{-1}/3 s (±10%)
Solar spectral flux	Spectrometer (380-1700 nm) with nadir and zenith hemispheric collectors	P. Pilewskie, U. of Colorado	Absolute accuracy 3-5%. Precision 1%/0.25 s

* Instruments on board the DC-8 and J-31 also measured pressure, temperature, dew point, aircraft position and orientation

Table 3. Satellite measurements targeted for validation in INTEX-A*

Satellite instruments	Platform (Launch date)	Validation measurements	More information
MISR	Terra	Aerosol	http://terra.nasa.gov/About/MISR/index.php
MODIS	(December 1999)	Aerosol, H_2O	http://terra.nasa.gov/About/MODIS/index.php
MOPITT		CO	http://terra.nasa.gov/About/MOPITT/index.php
AIRS	Aqua	CO, H_2O	http://aqua.nasa.gov/about/instrument_airs.php
MODIS	(May 2002)	Aerosol, H_2O	http://aqua.nasa.gov/about/instrument_modis_science.php
SCIAMACHY	Envisat (March 2002)	NO_2, HCHO	http://www.iup.physik.uni-bremen.de/sciamachy/

*All validations were performed with instruments looking in the nadir

Table 4. Models used for flight forecasting and analysis in INTEX-A*

Model	Type	Resolution		Underlying Meteorological Model	Chemical Package	P. I.	Additional References
		Horizontal	Vertical levels				
GEOS-4[1]	Global	1° x 1.25°	55	GEOS-4	Tagged tracers	D. J. Jacob, Harvard, U.	
GEOS-Chem	Global	2° x 2.5°	55	GEOS-4	Ozone-NO_x-VOC-aerosol chemistry	D. J. Jacob, Harvard, U.	Hudman et al. [this issue]
MOZART-4-GFDL	Global	1.9° x 1.9°	64	NCEP/GFS forecast	C_1-C_{10} detailed NMHC Chemistry; tagged tracers	L. W. Horowitz, NOAA/GFDL	Horowitz et al. [2003)
MOZART-4-NCAR	Global	2.8° x 2.8°	28	NCAR/NCEP Reanalysis	C_1-C_{10} detailed NMHC Chemistry; tagged tracers	L. K. Emmons, NCAR	Pfister et al. (2005]
RAQMS	Global	2° x 2.5°	36	NCEP	C_1-C_7 detailed NMHC Chemistry; tagged tracers	R. B. Pierce, NASA Langley	Pierce et al., [2003]
STEM	Regional	4 x 4 km to 80 x 80 km	21	MM5 or RAMS	C_1-C_7 detailed NMHC Chemistry; tagged tracers	G. R. Carmichael, Univ. of Iowa	Tang et al. [2004]
Photochemical Model/LaRC	Box	--	--	--	C_1-C_7 detailed NMHC Chemistry	J. H. Crawford NASA Langley	Crawford et al. [1999]

* Flight planning process also used weather forecasts based on NCEP analysis and near real-time satellite data from AIRS and MOPITT (CO columns), MODIS and AVHRR (aerosol, fire counts), TOMS (tropospheric ozone, absorbing aerosols), and LIS (lightning). Potential vorticity and convective influence plots were also available.

Table 5A: INTEX-A DC-8 missions and salient activity *

Flight No.	Date	Operational Base#	Flight hours	Salient mission activity
1-2	6/26-29/2004	NASA Dryden Flight Research Center (DFRC)	10.5	Test Flights-No chemical data archival required
3	7/01/2004	NASA DFRC	8.5	AIRS** validation, characterization of low-level California and high level Asian outflow, background and inflow characterization, and stratospheric intrusions
4	7/06/2004	NASA DFRC to Mid-America Airport	7.4	California plume transported to the east, Arizona fire plumes, frontal crossings over midwest and convective outflow over Great Plains
5	7/8/2004	Mid-America Airport	8.9	Validation of the MOPITT and MODIS instruments aboard the Terra satellite, characterization of aged California outflow, mapping of mid-western boundary layer pollution, sampling of deep convection over the Carolinas, and exploring the relationship between biogenic emissions and their products over the Smoky Mountains
6	7/10/2004	Mid-America Airport	8.7	Validation of instruments aboard the Envisat (SCIAMACHY) and Aqua (AIRS, MODIS) satellites, mapping of mid- western boundary layer pollution, sampling of deep convection, exploring the relationship between biogenic emissions and their products, and characterization of outflow from Texas
7	7/12/2004	Mid-America Airport	9.1	Boundary layer mapping of south-central U.S., aged convective/lightning outflow over southeast U.S. and validation of Park Falls FTS, SCIAMACHY, and AIRS
8	7/15/2004	Mid-America Airport to Pease International Tradeport Airport (ITA)	7.5	Validation of Terra (MOPITT, MISR) and Aqua (AIRS, MODIS) instruments, validation of FTS CO2 column measurements at Park Falls, CO2 inter- comparison with the NSF King Air aircraft, characterization of Asian pollution, Alaskan fires, and anthropogenic pollution
9	7/18/2004	Pease ITA	9.1	Validation of Envisat (SCIA) and Aqua (AIRS, MODIS) satellite instruments, a first attempt at the Lagrangian experiment, characterization of North American pollution outflow, characterization of Alaskan fires, and a flyby over the NOAA ship Ron Brown
10	7/20/2004	Pease ITA	7.9	Validation of Aqua (AIRS, MODIS)instruments, characterization of smoke from Alaskan fires transported over the US, boundary layer pollution over the southeast and mid- west,and a coordinated radiation closure experiment with the J-31
11	7/22/2004	Pease ITA	8.9	Sampling polluted boundary layer outflow along the eastern seaboard both to the north and south of Pease. Intercomparison between the NASA DC-8 and NOAA WP-3D aircraft. A coordinated validation profile with the J-31 over the NOAA research vessel Ron Brown and beneath the MISR instrument on NASA's Terra satellite.
12	7/25/2004	Pease ITA	9.3	Convective outflow from southeast US, map Ohio River Valley emissions in northerly flow and Terra underflight.
13	7/28/2004	Pease ITA	10.2	Sample the structure and chemical evolution of the US continental outflow over the Atlantic and a comparison between the measurements on the DC-8 and the BAe146.

14	7/31/2004	Pease ITA	9.0	Satellite underpass, aged air sampling/recirculation, low level outflow, DC-8/P-3 inter-comparison, and possible Asian influences
15	8/02/2004	Pease ITA	9.5	Under-fly Terra (MOPITT/MODIS) and Aqua (AIRS) satellites, sample low level North American outflow and aged air pollution aloft, conduct a coordinated closure experiment over Ron Brown with the J-31, and a flyby over the ground Appledore island air quality station.
16	8/06/2004	Pease ITA	9.4	Continental outflow, city plumes, boundary layer characterization, Terra underflight
17	8/07/2004	Pease ITA	8.5	Under-fly Terra (MOPITT/MISR) and perform a predefined maneuver in coordination with the J-31, Ron Brown and MISR, sample North American outflow, a stratospheric intrusion, and perform P-3 intercomparison.
18	8/11/2004	Pease ITA to Mid-America Airport	8.5	Terra underpass, Aqua underpass, NA outflow and WCB lifting, frontal crossing and low level pollution
19	8/13/2004	Mid-America Airport	8.6	Satellite underpass and outflow from major industrial cities
20	8/14/2004	Mid-America Airport to NASA DFRC	7.9	Satellite underpass, Asian outflow, and NA inflow

* More details on individual flights can be found at http://cloud1.arc.nasa.gov/intex-na/flight_reps.html

[#] NASA DFRC: 34.9° N, 117.9° W; Mid-America Airport: 38.5° N, 89.8° W; Pease ITA: 43.1° N, 70.8° W

** AIRS: Atmospheric Infrared Sounder; MISR: Multiangle Imaging SpectroRadiometer; MOPITT: Measurement of Pollution in the Troposphere; MODIS: Moderate Resolution Imaging Spectroradiometer; SCIAMACHY: Scanning Imaging Absorption Spectrometer for Atmospheric Chartography

Table 5B- INTEX-A J-31 missions and salient activity*

Flight No.	Date	Flight hours	Salient mission activity
1-3	05/13/2004 & 07/9/2004	3.8	Three test flights near NASA Ames
4-6	7/10/2004	11.9	Three flights to transit Ames to Pease
7	07/12/2004	2.9	Aqua overpass at 1813 UT; good profile data, RV Ron Brown rendezvous
8	07/15/2004	3.0	Over stratus clouds near Ron Brown Terra overpass (1525 UT) and near surface Aqua (1705 UT); 2nd run above cloud past RB. 2 Ron Brown sondes
9	07/16/2004	3.1	Spiral descent and low level legs around Aqua overpass time (17:48UT), increasing fog in the vicinity of low level legs, profile near Ron Brown for special sonde.
10	07/17/2004	2.2	Spiral descent and low level legs around Terra overpass time (15:13UT), increasing Cirrus (Ci), about 5 minutes of Ci-free data, found Ron Brown under Ci
11	07/20/2004	2.3	Radiation legs over stratus near Ron Brown with Terra overpass in MISR local mode swath. AOD profiles over stratus. Brief AOD near surface
12	07/21/2004	2.7	Low-level runs during Aqua OP at 18:06UT, two profiles in clear. Aerosol gradient at several altitudes
13	07/22/2004	2.8	Coordination with DC-8, Ron Brown, and Terra in MISR local mode patch, collocated profile with DC-8 (18 min. apart) over Ron Brown
14	07/23/2004	1.9	Aerosol profiles and near-surface legs with Aqua (1754 UT).
15	07/26/2004	2.0	Meteo and H_2O profiles over Ron Brown near shore. Cirrus or lower clouds for most of flight
16	07/29/2004	3.9	Spiral descent profile over Ron Brown, multiple low level flybys of Ron Brown, Terra MISR local mode, Aqua, 2 Ron Brown sondes. Aerosol gradient 2 ways.
17	07/29/2004	4.3	Successful airborne Langley flight at constant press alt (~6.4 km GPS) at sunset.
18	07/31/2004	4.3	Flew 297 nm E of Pease to find cirrus-free air. Flew L-pattern at max alt of 20k ft, spiral down to 2k ft (stratus below), another L-pattern at 2k ft, and a final L-pattern at 7.5k ft above an aerosol layer. Upon return, descent above Ron Brown (3 mi offshore). Ron Brown sonde. Coordination with DC-3 lidar over Ron Brown, but AATS got water vapor data only, because of cirrus.
19	08/02/2004	2.5	Terra overpass. Profile and legs in clear area. Aerosol gradient two ways.
20	08/02/2004	4.4	Airborne Langley before descent to 200', then low level leg to Ron Brown, ascent over Ron Brown with its sonde, and continuation of airborne Langley
21	08/03/2004	2.4	Coordination w/DC-3 w/legs at ~200' and ~5200', followed by Ron Brown flyby and spiral ascent nearby with Ron Brown sonde.
22	08/07/2004	3.5	Coordination w/DC-8, Ron Brown & its sonde during Terra MISR local mode overpass. Includes 5000' and 200' L-shaped legs and RB flybys, and spiral ascent w/DC-8.

23	08/07/2004	5.0	Airborne Langley before/after descent and ascent in clear air just east of Ron Brown (~68.75W, 43N). Post Ron Brown Langley measurements were ENE of Ron Brown. Ron Brown sonde
24	08/08/2004	2.2	Aqua overpass at 1354 UT; very low AOD along extended 220' run from 70W to 68W, 42.75N; profiles down/up to 11,000'; level leg at 11,000'; ramped descent from 68W to ~69W
25	08/08/2004		Aborted on runway.
26	08/08/2004	3.0	Airborne Langley E of Pease

* All J-31 science flights originated from the Pease ITA (43.1° N, 70.8° W). These are daytime flights. More details on individual flights can be found at http://cloud1.arc.nasa.gov/intex-na/flight_reps.html

Table 6: Principal DC-8 airborne inter-comparisons

Intercomparing platforms	Dates (2004)	Approx location	Time (UT)[$]	Level altitude legs (km)*
DC-8 and King Air	7/15	46°N; 90°W	14:15-15:15	Spiral[#]
DC-8 and WP-3D	7/22	42°N; 68°W	14:45-15:30	4.4, 0.3
DC-8 and BAe146**	7/28	38°N; 38°W	15:50-17:02	6.8, 3.8, 0.2
DC-8 and WP-3D	7/31	45°N; 69°W	22:52-23:32	3.1, 0.6
DC-8 and WP-3D	8/07	44°N; 68°W	21:33-22:20	3.8, 0.3

* Aircrafts flew in formation for the entire time during level legs, descent, and/or ascent.
** The BAe146 also separately inter-compared with the DLR falcon
[#] Centered on the WLEF Tall Tower, the DC-8 and the King Air spiraled down from 11 to 0.1 km and 8 to 0.1 km respectively.

Table 7: Satellite validation opportunities during INTEX-A

Satellite Underflown	Flight	Dates (2004)	Approx location	Time (UT)
Aqua	3	7/1	41˚N; 127˚W	21:28-21:56
Terra	5	7/8	42˚N; 90˚W	17:21-17:55
Envisat	6	7/10	41˚N; 80˚W	15:53-16:22
Aqua	6	7/10	35˚N; 83˚W	18:22-18:55
Envisat	7	7/12	46˚N; 90˚W	16:21-16:47
Aqua	7	7/12	36˚N; 97˚W	19:27-19:52
Terra	8	7/15	46˚N; 90˚W	17:23-17:50
Envisat	9	7/18	47˚N; 63˚W	14:46-15:21
Aqua	9	7/18	48˚N; 55˚W	16:19-16:51
Aqua	10	7/20	41˚N; 90˚W	18:55-19:26
Terra	11	7/22	43˚N; 70˚W	15:58-16:36
Terra	12	7/25	28˚N; 79˚W	16:29-16:58
Aqua/Terra/Envisat	14	7/31	41˚N; 66˚W	16:01-16:27
Aqua/Terra	15	8/2	50˚N; 61˚W	16:21-16:48
Terra	16	8/6	36˚N; 84˚W	16:24-16:54
Terra	17	8/7	42˚N; 68˚W	15:20-15:46
Terra	18	8/11	37˚N; 65˚W	15:02-15:30
Aqua	18	8/11	37˚N; 83˚W	18:34-19:10
Terra	19	8/13	30˚N; 89˚W	15:37-16:14
Aqua	19	8/13	29˚N; 91˚W	18:51-19:50